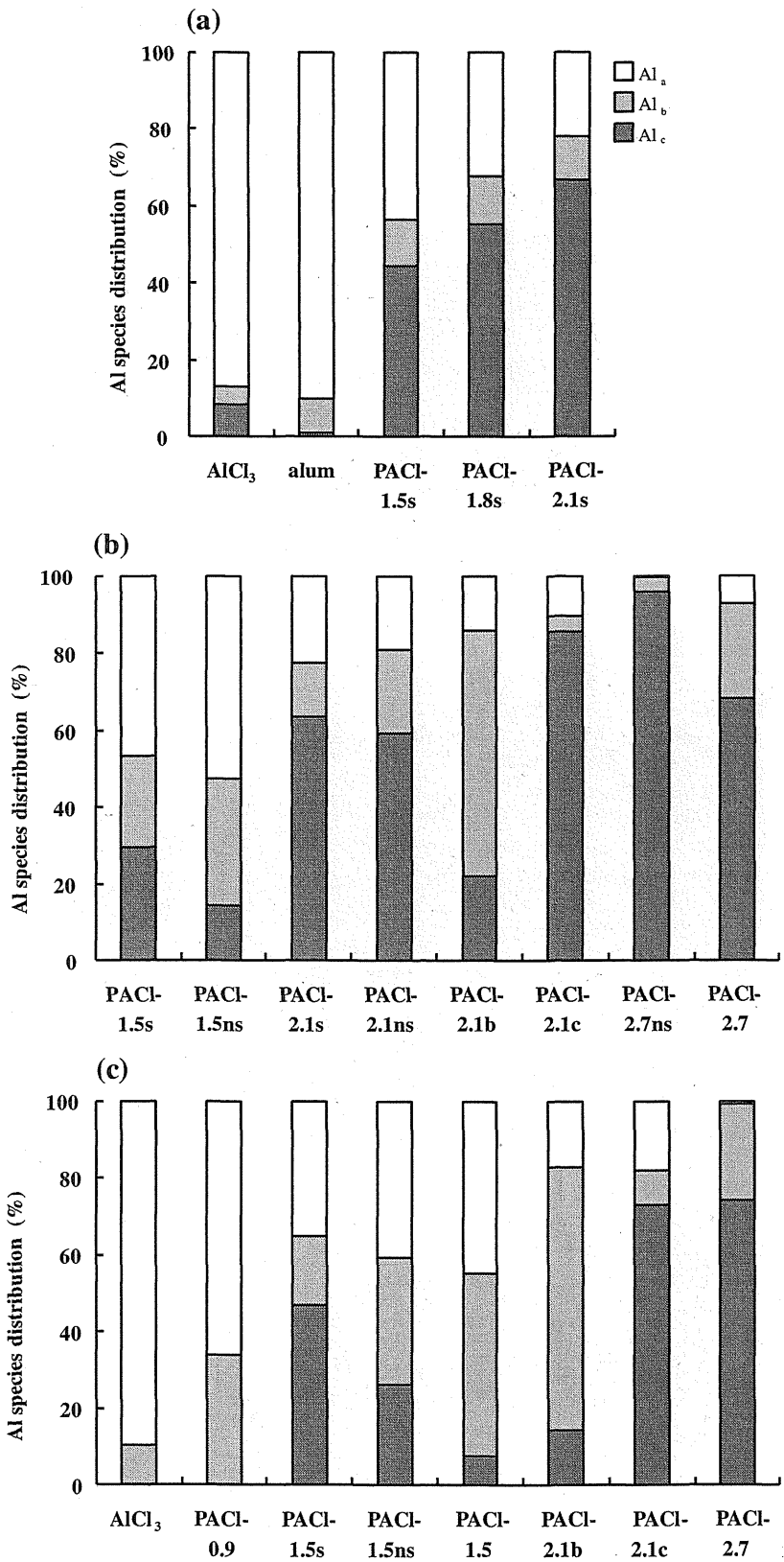

Fig. 4 – Distribution of aluminum species in the coagulants used in the first (a), second (b), and third (c) sets of experiments, as evaluated by the ferron method.

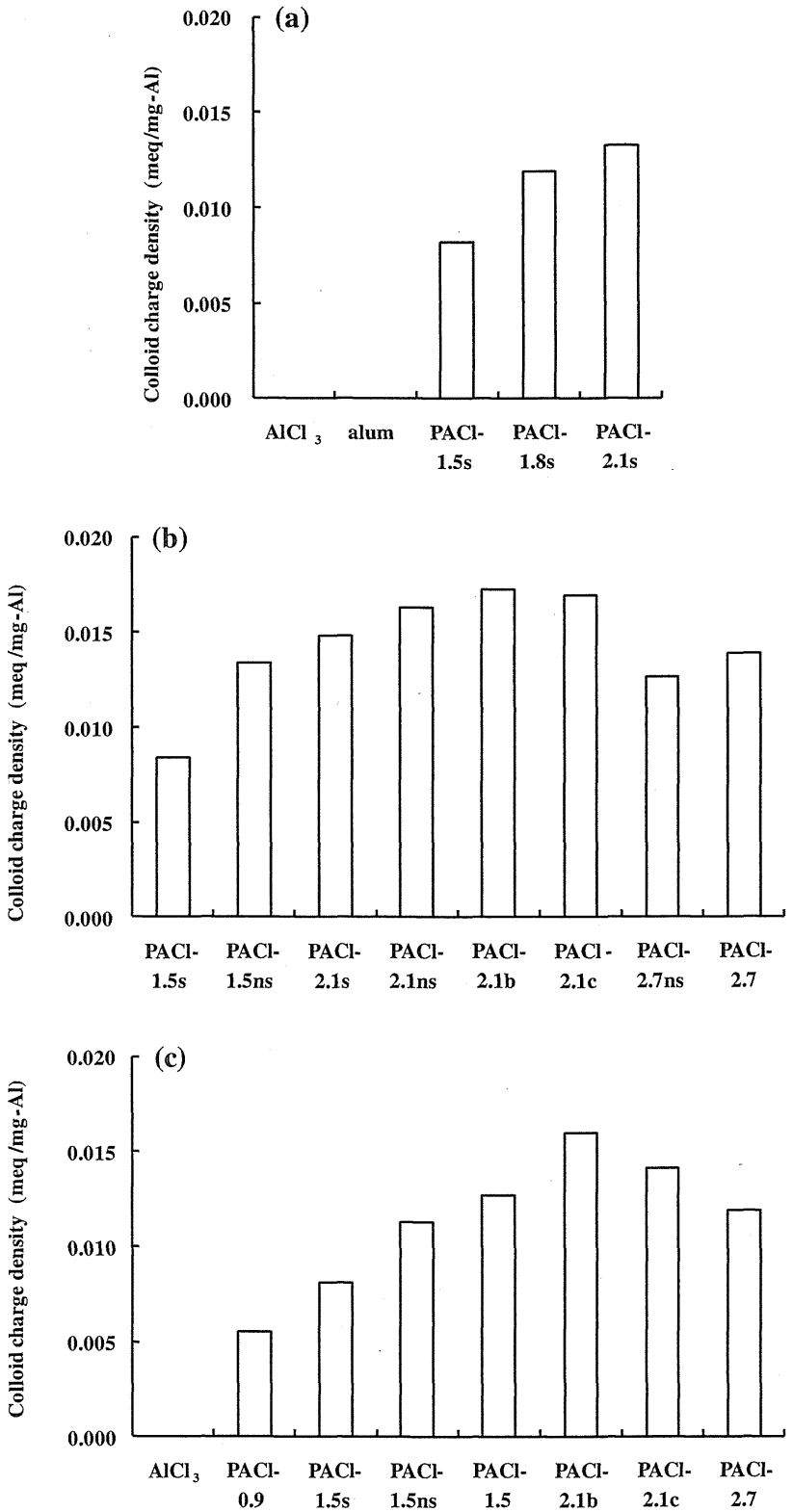

Fig. 5 – Colloid charges densities of the coagulants used in the first (a), second (b), and third (c) sets of experiments, as evaluated by a colloid titration technique.

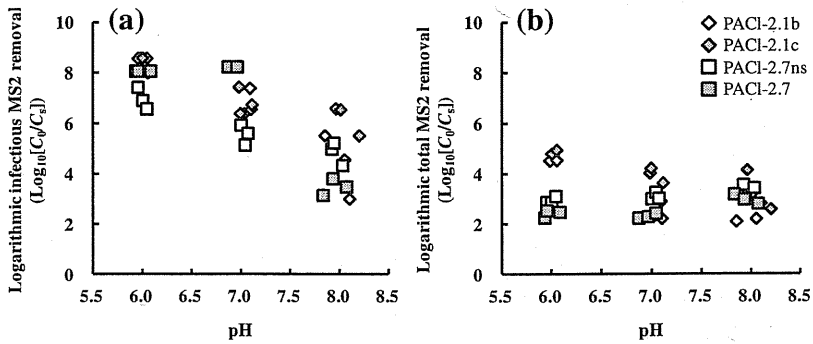

Fig. 6 – Effect of the aluminum hydrolyte species in the coagulants on infectious MS2 removal as evaluated by the PFU method (a) and on total MS2 removal as evaluated by the PCR method (b) after settling during the coagulation process. The source water was river water 2, and the coagulant dosage was 1.89 mg-Al/L.

with various sulfated and nonsulfated PACls and evaluated the infectious MS2 removal ratios by means of the PFU method after settling (Fig. 3a). Although no removal of infectious MS2 was observed in the absence of coagulant at any pH, as was the case for Qβ (data not shown), the coagulation process with PACl did remove infectious MS2, and the removal efficiency increased with increasing PACl basicity under all pH conditions. In addition, nonsulfated PACls removed infectious MS2 more efficiently than did sulfated PACls, regardless of their basicity: the infectious MS2 removal ratios during the coagulation process with PACl-1.5ns and PACl-2.1ns were approximately 1–4-log_{10} larger than the ratios with PACl-1.5s and PACl-2.1s, although the removal ratios observed with PACl-2.1s and PACl-2.1ns were almost same at around pH 7. The total MS2 removal ratios evaluated by the PCR method were also observed to be somewhat larger with nonsulfated PACls than the ratios with sulfated PACls, especially at around pH 8 (Fig. 3b). These results indicate that the sulfate in the PACls affected virus removal performance and that a nonsulfated high-basicity PACl (PACl-2.1ns) removed the virus more effectively than PACl-1.5s, PACl-1.5ns, and PACl-2.1s, not only under weakly acidic and neutral pH conditions but also at weakly alkaline pH.

To determine why PACl-2.1ns effectively removed viruses, we used the ferron method to investigate the distribution of aluminum species in the coagulants (Fig. 4). Whereas the major aluminum species in $AlCl_3$ and alum was monomeric aluminum species (Al_a), colloidal aluminum species (Al_c) were present in high proportions in the PACls (Fig. 4a). In addition, the Al_c content in the PACls increased and the Al_a content decreased with increasing basicity, whereas the content of polymeric aluminum species (Al_b) remained almost constant (Fig. 4a). The Al_{13} species $[AlO_4Al_{12}(OH)_{24}(H_2O)_{12}]^{7+}$ is generally believed to be the most effective aluminum species for coagulation processes, because of its strong charge neutralization capability and structural stability (Chen et al., 2006); and the amount of Al_{13} species in a coagulant is almost equivalent to the amount of Al_b measured by the ferron method (Chen et al., 2007). In the present study, the virus removal performances of PACl-1.5s, PACl-1.5ns, PACl-2.1s, and PACl-2.1ns differed markedly, especially at weakly alkaline pH, even though their Al_b contents were not substantially different (Fig. 4b). Therefore, Al_b, including Al_{13} species, may not have been the dominant species responsible for controlling virus removal performance during the coagulation process.

The Al_{30} species $[Al_{30}O_8(OH)_{56}(H_2O)_{24}]^{18+}$ is known to be an effective aluminum species for coagulation processes, and some researchers have demonstrated that PACls with a high Al_{30} content remove more turbidity and more humic acid than PACls with a high Al_{13} content (Chen et al., 2006; Zhang et al., 2008). Because Al_{30} species do not react with the ferron reagent within 120 min, they are categorized as Al_c by the ferron method (Chen et al., 2007). We found that PACl-2.1s and PACl-2.1ns had higher Al_c contents and lower Al_a contents than $AlCl_3$, alum, PACl-1.5s, PACl-1.5ns, and PACl-1.8s (Fig. 4a,b). Therefore, Al_c, including Al_{30} species, may have been the dominant species controlling virus removal performance during the coagulation process. Our investigation of the effects of the Al_b and Al_c contents in the coagulants on virus removal is discussed in Section 3.2.2.

We observed no large differences between the distributions of aluminum species in the sulfated and nonsulfated PACls. These results suggest that PACl basicity affected aluminum species distributions but that the presence of sulfate in the PACls did not.

We also determined the positive colloid charge densities of the coagulants by using a colloid titration technique (Fig. 5). The colloid charge densities of $AlCl_3$ and alum were very small and almost zero; those of the PACls increased with increasing basicity, and PACl-2.1s and PACl-2.1ns showed higher colloid charge densities than $AlCl_3$, alum, PACl-1.5s, PACl-1.5ns, and PACl-1.8s (Fig. 5a,b). In addition, the colloid charge densities of the nonsulfated PACls were higher than those of the sulfated PACls. Wang et al. (2002) reported that the presence of sulfate during the coagulation process reduces the charge neutralization capability of coagulants; this reduction is due to the moderate interaction of sulfate with aluminum hydrolyte species and aluminum hydroxide. Nevertheless, sulfate is often added to aluminum-based coagulants to broaden the pH range of optimum destabilization (i.e., acceleration of floc formation) to the acidic side (Hanna and Rubin, 1970). Therefore, the high Al_c content and the absence of sulfate in PACl-2.1ns probably led to the increased colloid charge density, which gave this coagulant its high

capability to neutralize the negative charge on the viruses during the coagulation process.

3.2.2. *Effect of aluminum species in coagulants on bacteriophage removal*

To investigate the effect of the nature of the aluminum species in the coagulants on virus removal, we compared the MS2 removal efficiencies of nonsulfated high-basicity PACl-2.1b and PACl-2.1c, whose predominant aluminum hydrolyte species are Al_b and Al_c, respectively. PACl-2.1b and PACl-2.1c removed infectious MS2 at a pH range of 6–7 with nearly identical removal efficiencies (~6–7-log_{10} removal), as evaluated by means of the PFU method (Fig. 6a). In contrast, at around pH 8, the infectious MS2 removal ratio observed with PACl-2.1c was approximately 2-log_{10} larger than that with PACl-2.1b. The total MS2 removal ratios evaluated by means of the PCR method were also observed to be somewhat larger with PACl-2.1c than the ratios with PACl-2.1b at around pH 7 and 8 (Fig. 6b). These results indicate that the distribution of aluminum species in the PACls affected virus removal performance during the coagulation process and that Al_c-dominant PACl (i.e., PACl-2.1c) was particularly effective at removing the virus at weakly alkaline pH. Our hypothesis that coagulants with high Al_c content effectively removed viruses during the coagulation process is supported by these results.

To identify the aluminum hydrolyte species in PACl-2.1b and PACl-2.1c, we analyzed the coagulants by ^{27}Al NMR in addition to the ferron method. In the ^{27}Al NMR spectra of all the coagulants, two or three signals were observed (Fig. 7): the signals at 0, 63, and 80 ppm were attributed to monomeric species (Al_m), the central tetrahedral Al in Al_{13} species, and the internal standard (that is, to the formation of $[Al(OH)_4]^-$), respectively (Chen et al., 2006, 2007; Gao et al., 2005; Liu et al., 2009). Whereas no signal or only a weak signal for Al_{13} species was confirmed in the spectra of $AlCl_3$ and PACl-1.5s, a strong signal for this species was observed in the spectrum of PACl-2.1b (Fig. 7). Because the MS2 removal ratios observed with PACl-2.1b were markedly larger than those with PACl-1.5s (Figs. 3 and 6), we suggest that Al_{13} species in PACl are among the important species controlling virus removal performance during the coagulation process. Although a signal for Al_{13} species was also observed for PACl-2.1c, the intensity of the signal was lower than that for PACl-2.1b. This result suggests that the Al_{13} content in PACl-2.1b was higher than that in PACl-2.1c (Fig. 7). This observation is in accord with the results obtained by the ferron method, which indicate that the predominant aluminum hydrolyte species in PACl-2.1b was Al_b and that the Al_{13} species in coagulant are almost equivalent to that of Al_b, as described above.

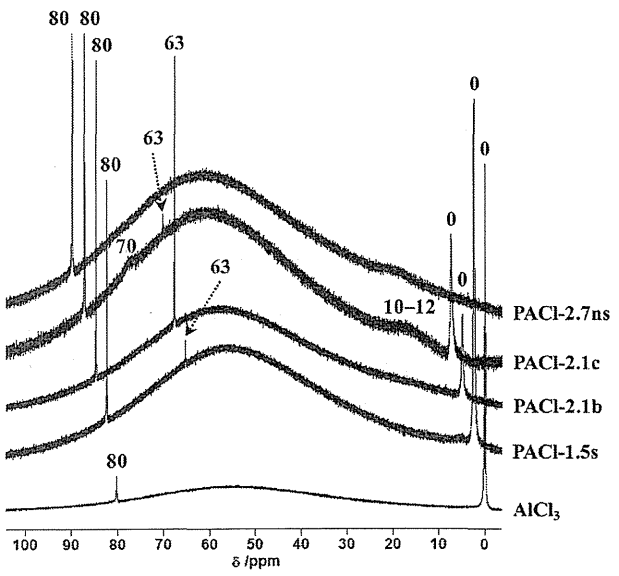

Fig. 7 – ^{27}Al NMR spectra of coagulants used in the second set of experiments.

In addition to the signals at 0, 63, and 80 ppm, the spectrum of PACl-2.1c showed broad signals at 10–12 and 70 ppm, which were attributed to the octahedral Al of external shells in Al_{13} and Al_{30} species and the central tetrahedral Al in Al_{30} species, respectively (Chen et al., 2007). This result indicates that PACl-2.1c contained not only Al_{13} species but also Al_{30} species, which was not the case for PACl-2.1b. In addition, Al_{30} species played the major role in virus removal, as indicated by the fact that the efficiency of MS2 removal with PACl-2.1c was somewhat larger than that with PACl-2.1b (Fig. 6), even though the Al_{13} content in PACl-2.1c was smaller than that in PACl-2.1b (Fig. 7). Although the Al_m (Al_a) species contributed to virus removal—as indicated by the fact that high-Al_m-content coagulants ($AlCl_3$ and PACl-1.5s) removed some virus at a pH range of 6–7, probably because of the formation of Al_{13} (Al_b) species in situ (Hu et al., 2006; Yan et al., 2008a)—conversion of Al_m species in the coagulant to Al_{13} species and further transformation of Al_{13} species into Al_{30} species effectively improved virus removal performance during the coagulation process.

We further investigated the effect of the aluminum species in the coagulants on virus removal by evaluating two extremely high basicity PACls (i.e., PACl-2.7ns and PACl-2.7). The efficiencies of infectious MS2 removal at a pH range of 6–7, as evaluated by the PFU method after settling, were 6–8-log_{10} (Fig. 6a). These removal ratios were similar to the ratio obtained with PACl-2.1c. In contrast, the ratios observed with PACl-2.7ns and PACl-2.7 were approximately 1–3-log_{10} smaller than the ratio with PACl-2.1c at around pH 8. The total MS2 removal efficiencies, as evaluated by the PCR method, during the coagulation process with extremely high basicity PACls were also similar to or somewhat smaller than the ratio observed with PACl-2.1c (Fig. 6b). The effective removal of turbidity and UV260-absorbing NOM, and the very low residual aluminum concentration, observed in the coagulation process with PACl-2.7ns and PACl-2.7 were attained not only under weakly acidic and neutral pH conditions but also at weakly alkaline pH compared with other aluminum-based coagulants used in the present study, including PACl-2.1c (Fig. S2). However, increasing the PACl basicity from 2.1 to 2.7 was not effective for virus removal, even though the Al_c content in PACl-2.7ns was larger than that in PACl-2.1c (Fig. 4b). Moreover, we observed a reduction of the colloid charge densities of the PACls when the basicity was increased from 2.1 to 2.7 (Fig. 5b,c), and no signal for Al_{30} species was observed in the ^{27}Al NMR spectrum of PACl-2.7ns (Fig. 7). The reason why the colloid charge densities of the coagulants were reduced by the increase in basicity is not clear, but these

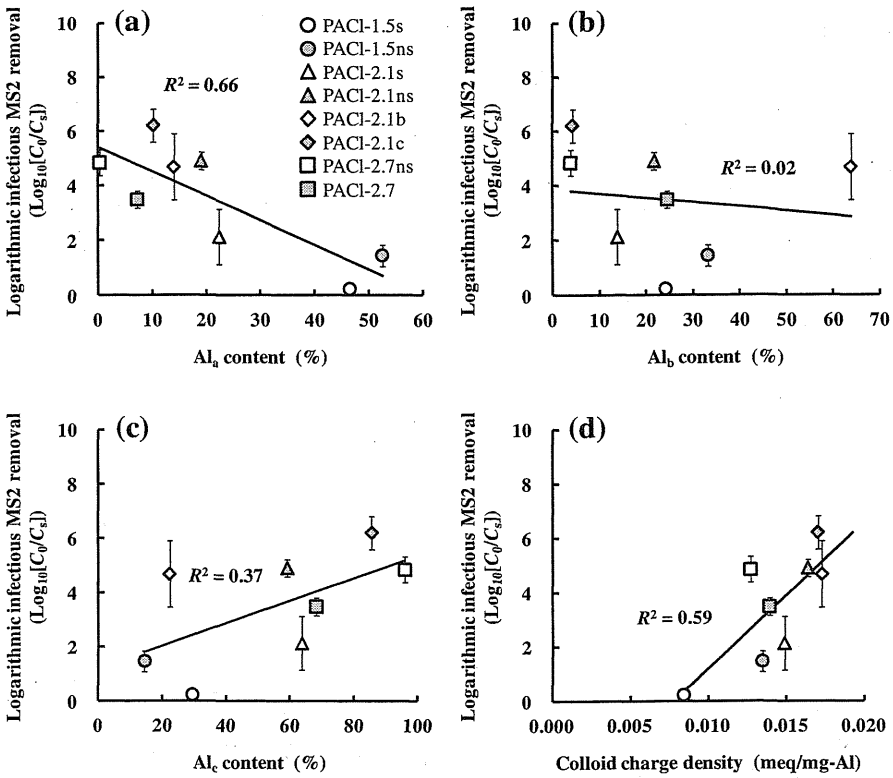

Fig. 8 – Relationship between infectious MS2 removal ratios and Ala (a), Alb (b), Alc (c), and colloid charge density (d). The source water was river water 2, and the coagulant dosage was 1.89 mg-Al/L. The pH of the treated water was approximately 8. Values are means (n = 3–4), and the error bars indicate standard deviations.

results suggest that virus removal efficiency during the coagulation process with PACls was not determined simply by the amount of Al_c in the coagulants.

3.2.3. *Relationship between bacteriophage removal, aluminum species and colloid charge density*

In our previous study, we found that the amount of Al_a in PACls, rather than their basicity, was a better indicator to use for minimizing residual aluminum concentration after settling at weakly alkaline pH (Kimura et al., 2013). To investigate whether the Al_a, Al_b, or Al_c content or the colloid charge density of the coagulants could be used as an indicator for the effectiveness of virus removal during the coagulation process, we determined the relationships between the MS2 removal ratio at around pH 8 and the Al_a, Al_b, and Al_c contents and the colloid charge density (Fig. 8). There was no correlation between the efficiency of infectious MS2 removal and the Al_b and Al_c contents; whereas the Al_a content, that is, [100% – (Al_b + Al_c)], and the colloid charge density were weakly correlated with the infectious MS2 removal ratios

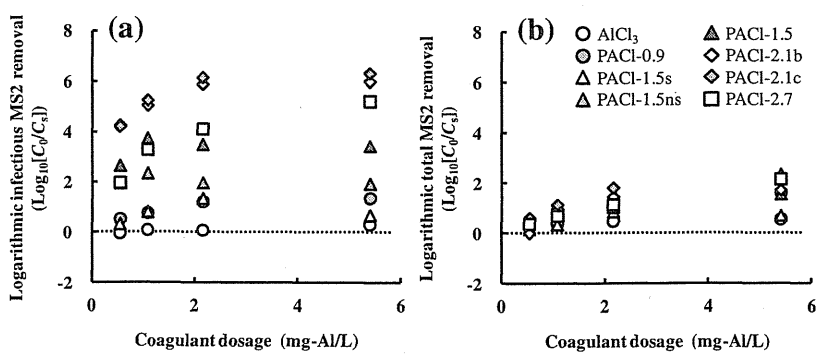

Fig. 9 – Effect of coagulant dosage on infectious MS2 removal as evaluated by the PFU method (a) and on total Qβ removal as evaluated by the PCR method (b) after settling during the coagulation process. The source water was river water 3, and the pH of the treated water was approximately 8.

(Fig. 8). In the third set of experiments (described below), the amount of Al_a, the colloid charge density, and both together were also correlated with the efficiency of infectious or total MS2 removal at all coagulant dosages, except for the total MS2 removal ratio at a coagulant dosage of 0.54 mg-Al/L (Table S4). In addition, the removal ratios tended to increase as the amount of Al_a in the PACls decreased (that is, as $Al_b + Al_c$ increased) and as the colloid charge density of the PACls increased. However, the virus removal efficiencies during the coagulation process with aluminum-based coagulants were not solely dependent on either $Al_b + Al_c$ or the colloid charge density. Further investigation is needed to elucidate a completely reliable indicator for the effectiveness of virus removal during the coagulation process.

3.3. *Third set of experiments*

3.3.1. *Effect of coagulant dosage on bacteriophage removal*

Fig. 9a shows the effect of coagulant dosage on the efficiency of infectious MS2 removal from treated water at around pH 8, as evaluated by means of the PFU method after settling. The infectious MS2 removal ratio increased as the coagulant dosage was increased from 0.54 to 2.16 mg-Al/L; although the removal ratios observed with $AlCl_3$ and PACl-1.5ns were unaffected by the increase in coagulant dosage, approximately 1–2-log_{10} improvements were obtained for the other aluminum-based coagulants. For most of the coagulants, the infectious MS2 removal ratio reached a maximum at a dosage of 2.16 mg-Al/L, and retained its virus removal performance when the coagulant dosage was further increased to 5.4 mg-Al/L, except in the case of PACl-1.5s. A similar trend was observed for removal of turbidity and UV260-absorbing NOM (Fig. S3). These results indicate that re-stabilization likely did not occur at this dosage range for any of the coagulants except PAC-1.5s.

The infectious MS2 removal ratios during the coagulation process with high-basicity PACls (i.e., PACl-2.1b, PACl-2.1c, and PACl-2.7) were larger than the ratios with the other aluminum-based coagulants used in the present study at all coagulant dosages. A similar trend was observed for the total MS2 removal ratios, as evaluated by the PCR method (Fig. 9b). Therefore, increasing coagulant basicity tended to lower the coagulant dosage required for effective removal of viruses. In addition, the coagulation process with PACl-2.1c removed MS2 more efficiently than the other aluminum-based coagulants at all coagulant dosages; PACl-2.1c was therefore useful for virus removal over a broader pH range and wider coagulant dosage range compared to commercially available aluminum-based coagulants.

3.3.2. *Overall comparison of coagulation efficiency of the tested coagulants*

As described above, PACl-2.1c, which contains Al_{30} species, removed viruses more efficiently than the other aluminum-based coagulants, especially at weakly alkaline pH. In contrast, at pH 8, the UV260-absorbing NOM removal and the residual aluminum concentration attained with PACl-2.7 were better than those attained with PACl-2.1c (Fig. S3). Because a low residual aluminum concentration is associated with a low content of monomeric aluminum species in the coagulant, our previously reported coagulation process with PACl-2.7 (Kimura et al., 2013), which has a low Al_a content (Fig. 4c), attained a very low residual aluminum concentration. Taken together, our results suggest that the development of novel aluminum-based coagulants for different purposes such as efficient virus removal and low residual aluminum concentration can be achieved. The experimental results obtained in the present study will be useful for the development and investigation of highly effective aluminum-based coagulants.

4. Conclusions

(1) An increase in PACl basicity (from 1.5 to 2.1) and the absence of sulfate in the PACls improved virus removal efficiency.
(2) The efficiency of virus removal at around pH 8 observed with PACl-2.1c, a nonsulfated high-basicity PACl with a high Al_c content, was larger than that with PACl-2.1b, a nonsulfated high-basicity PACl with a high Al_b content.
(3) Although extremely high basicity PACls (PACl-2.7ns and PACl-2.7) effectively removed turbidity and UV260-absorbing NOM and resulted in a very low residual aluminum concentration, the virus removal ratios of these two PACls were smaller than the ratio with PACl-2.1c at around pH 8, possibly as a result of a reduction in the colloid charge density of the PACl due to the increase in basicity from 2.1 to 2.7.
(4) Al_{30} species probably played the major role in virus removal during the coagulation process.
(5) Among the various aluminum-based coagulants used in the present study, PACl-2.1c, which has a high Al_c content (including Al_{30} species) and a high colloid charge density, showed the highest virus removal ratio (>4 log_{10} for infectious viruses) in the pH range from 6 to 8 and a coagulant dosage range from 0.54 mg-Al/L to 5.4 mg-Al/L.
(6) The virus removal ratios tended to increase as the amount of Al_a in the coagulant decreased (that is, as $Al_b + Al_c$ increased) and as the colloid charge density of the coagulant increased.

Acknowledgments

This research was supported in part by a Grant-in-Aid for Young Scientists A (no. 25709044, 2013), a Grant-in-Aid for Scientific Research S (no. 24226012, 2012), and a Grant-in-Aid for Scientific Research B (no. 24360211, 2012) from the Japan Society for the Promotion of Science; by a Grant-in-Aid (2013) from the Ministry of Health, Labor and Welfare of Japan; by the Kurita Water and Environment Foundation (no. 23050, 2011); and by the Japan Prize Foundation (2012).

Appendix A. Supplementary material

Supplementary material associated with this article can be found, in the online version, at http://dx.doi.org/10.1016/j.watres.2013.09.052.

REFERENCES

Adams, M.H., 1959. Bacteriophages. Interscience Publishers, New York, NY, USA, pp. 450–454.

Boudaud, N., Machinal, C., David, F., Bourdonnec, A.F.L., Jossent, J., Bakanga, F., Arnal, C., Jaffrezic, M.P., Oberti, S., Gantzer, C., 2012. Removal of MS2, Qβ and GA bacteriophages during drinking water treatment at pilot scale. Water Res. 46 (8), 2651–2664.

Bratby, J., 2006. Coagulation and Flocculation in Water and Wastewater Treatment, second ed. IWA Publishing, London, UK, pp. 80–86. 114–115.

Chen, Z., Fan, B., Peng, X., Zhang, Z., Fan, J., Luan, Z., 2006. Evaluation of Al_{30} polynuclear species in polyaluminum solutions as coagulant for water treatment. Chemosphere 64 (6), 912–918.

Chen, Z., Luan, Z., Fan, J., Zhang, Z., Peng, X., Fan, B., 2007. Effect of thermal treatment on the formation and transformation of Keggin Al_{13} and Al_{30} species in hydrolytic polymeric aluminum solutions. Colloids Surf. A: Physicochem. Eng. Aspects 292 (2–3), 110–118.

Fauquet, C.M., Mayo, M.A., Maniloff, J., Desselberger, U., Ball, L.A. (Eds.), 2005. Virus Taxonomy: Eighth Report of the International Committee on Taxonomy of Viruses. Elsevier Academic Press, London, UK, pp. 741–750.

Fiksdal, L., Leiknes, T., 2006. The effect of coagulation with MF/UF membrane filtration for the removal of virus in drinking water. J. Membr. Sci. 279 (1–2), 364–371.

Gao, B.Y., Chu, Y.B., Yue, Q.Y., Wang, B.J., Wang, S.G., 2005. Characterization and coagulation of a polyaluminum chloride (PAC) coagulant with high Al_{13} content. J. Environ. Manage. 76 (2), 143–147.

Guo, H., Hu, J.Y., 2011. Optimization study of a hybrid alum coagulation-membrane filtration system for virus removal. Water Sci. Technol. 64 (9), 1843–1850.

Hanna, G.P., Rubin, A.J., 1970. Effect of sulfate and other ions in coagulation with aluminum (III). J. Am. Water Works Assoc. 62 (5), 315–321.

Hijnen, W.A.M., Medema, G.J., 2010. Elimination of Micro-organisms by Water Treatment Processes. IWA Publishing, London, UK, pp. 23–34.

Hu, C.Z., Liu, H.J., Qu, J.H., Wang, D.S., Ru, J., 2006. Coagulation behavior of aluminum salts in eutrophic water: significance of Al_{13} species and pH control. Environ. Sci. Technol. 40 (1), 325–331.

Kimura, M., Matsui, Y., Kondo, K., Ishikawa, T., Matsushita, T., Shirasaki, N., 2013. Minimizing residual aluminum concentration in treated water by tailoring properties of polyaluminum coagulants. Water Res. 47 (6), 2075–2084.

Liu, H.J., Hu, C.Z., Zhao, H., Qu, J.H., 2009. Coagulation of humic acid by PACl with high content of Al_{13}: the role of aluminum speciation. Sep. Purif. Technol. 70 (2), 225–230.

Matsui, Y., Matsushita, T., Sakuma, S., Gojo, T., Mamiya, T., Suzuoki, H., Inoue, T., 2003. Virus inactivation in aluminum and polyaluminum coagulant. Environ. Sci. Technol. 37 (22), 5175–5180.

Matsukawa, S., Itoho, S., Habuthu, S., Aizawa, T., 2006. An approach to residual aluminium control at Nisiya purification plant, Water Works Bureau, Yokohama. Water Sci. Technol. Water Supply 6 (4), 67–74.

Matsushita, T., Shirasaki, N., Matsui, Y., Ohno, K., 2011. Virus inactivation during coagulation with aluminum coagulants. Chemosphere 85 (4), 571–576.

Nasser, A., Weinberg, D., Dinoor, N., Fattal, B., Adin, A., 1995. Removal of hepatitis A virus (HAV), poliovirus and MS2 coliphage by coagulation and high rate filtration. Water Sci. Technol. 31 (5–6), 63–68.

Pernitsky, D.J., Edzwald, J.K., 2003. Solubility of polyaluminium coagulants. J. Water Supply Res. Technol. AQUA 52 (6), 395–406.

Shirasaki, N., Matsushita, T., Matsui, Y., Urasaki, T., Ohno, K., 2009a. Comparison of behaviors of two surrogates for pathogenic waterborne viruses, bacteriophages Qβ and MS2, during the aluminum coagulation process. Water Res. 43 (3), 605–612.

Shirasaki, N., Matsushita, T., Matsui, Y., Kobuke, M., Ohno, K., 2009b. Comparison of removal performance of two surrogates for pathogenic waterborne viruses, bacteriophage Qβ and MS2, in a coagulation-ceramic microfiltration system. J. Membr. Sci. 326 (2), 564–571.

Shirasaki, N., Matsushita, T., Matsui, Y., Oshiba, A., Ohno, K., 2010. Estimation of norovirus removal performance in a coagulation-rapid sand filtration process by using recombinant norovirus VLPs. Water Res. 44 (5), 1307–1316.

Wang, D., Tang, H., Gregory, J., 2002. Relative importance of charge neutralization and precipitation on coagulation of kaolin with PACl: effect of sulfate ion. Environ. Sci. Technol. 36 (8), 1815–1820.

Wang, D., Sun, W., Xu, Y., Tang, H., Gregory, J., 2004. Speciation stability of inorganic polymer flocculant–PACl. Colloids Surf. A: Physicochem. Eng. Aspects 243 (1–3), 1–10.

Yan, M.Q., Wang, D.S., Qu, J.H., Ni, J.R., Chow, C.W.K., 2008a. Enhanced coagulation for high alkalinity and micro-polluted water: the third way through coagulant optimization. Water Res. 42 (8–9), 2278–2286.

Yan, M.Q., Wang, D.S., Yu, J.F., Ni, J.R., Edwards, M., Qu, H.H., 2008b. Enhanced coagulation with polyaluminum chlorides: role of pH/Alkalinity and speciation. Chemosphere 71 (9), 1665–1673.

Yang, Z.L., Gao, B.Y., Cao, B.C., Xu, W.Y., Yue, Q.Y., 2011. Effect of OH^-/Al^{3+} ratio on the coagulation behavior and residual aluminum speciation of polyaluminum chloride (PAC) in surface water treatment. Sep. Purif. Technol. 80 (1), 59–66.

Zhang, P., Wu, Z., Zhang, G., Zeng, G., Zhang, H., Li, J., Song, X., Dong, J., 2008. Coagulation characteristics of polyaluminum chlorides PAC-Al_{30} on humic acid removal from water. Sep. Purif. Technol. 63 (3), 642–647.

Zhu, B.T., Clifford, D.A., Chellam, S., 2005. Virus removal by iron coagulation-microfiltration. Water Res. 39 (20), 5153–5161.

Separation and Purification Technology 107 (2013) 79–84

Contents lists available at SciVerse ScienceDirect

Separation and Purification Technology

journal homepage: www.elsevier.com/locate/seppur

Adsorptive virus removal with super-powdered activated carbon

Taku Matsushita *, Hideaki Suzuki, Nobutaka Shirasaki, Yoshihiko Matsui, Koichi Ohno

Graduate School of Engineering, Hokkaido University, N13W8, Sapporo 060-8628, Japan

ARTICLE INFO

Article history:
Received 17 April 2012
Received in revised form 10 January 2013
Accepted 15 January 2013
Available online 31 January 2013

Keywords:
Bacteriophage
Drinking water treatment
Hydrophobicity
Zeta potential

ABSTRACT

We investigated the removal of bacteriophages by adsorption on commercially available powdered activated carbon (N-PAC, median diameter >10 μm) and super-powdered activated carbon (S-PAC, median diameter 0.7–2.8 μm). N-PACs failed to remove the virus in Milli-Q water buffered with 100 μM Ca^{2+}, but some S-PACs successfully removed it under the same condition. Three factors contributed substantially to virus removal: a smaller electrophoretic repulsive force between the virus and the PAC particles, a large proportion of pores 20–50 nm in diameter, and a greater hydrophobicity of the virus surface.

1. Introduction

The development of detection techniques based on molecular biology has enabled us to detect fragments of viral genomes in environmental waters, including drinking water sources, highlighting the need to ensure the removal of viruses at drinking water treatment plants. Although disinfecting water with hypochlorite ensures the biological safety of the finished water, the risk of virus infections can be reduced by physicochemical treatments such as coagulation–sedimentation–sand filtration; physical sieving processes such as ultrafiltration, nanofiltration, and reverse osmosis; and ozonation and UV irradiation.

Activated carbon adsorption is widely used to treat drinking water in Japan. Granular activated carbon (GAC) is used in combination with ozonation for removing byproducts derived from the oxidative decomposition of organic matter. Powdered activated carbon (PAC) is seasonally applied with excellent results for removing chemicals with an earthy–musty odor and pesticides. It has also been tested for virus removal. Adsorption experiments with a GAC-loaded (20 × 50 mesh, equivalent to 297–853 μm) column-type reactor removed only 24–50% of poliovirus [1]. Worse, GAC filtration did not remove bacteriophage MS2 [2]. These results indicate that GAC is not suitable for substantial virus removal within the contact time allowed in actual drinking water treatment, probably on account of a low rate of adsorption of virus. Indeed, only 70% of bacteriophage T4 was removed by activated carbon (300–425 μm) after 2 h of contact time [3]. Accordingly, effective virus removal by activated carbon will require a longer contact time, an extremely high dose of activated carbon, or both.

Reducing the particle size of activated carbon increases the rate of adsorption [4,5], because the travel distance for intraparticle radial diffusion is reduced and the specific surface area per adsorbent mass is increased [6]. Pulverizing activated carbon would therefore overcome the problems of slow adsorption kinetics, but the PAC particle size was previously limited to about 5 μm. Recent advances in nanotechnology now enable pulverization down to submicron or nanometer size ranges at a reasonable cost, producing super-powdered activated carbon (S-PAC) [7–9]. As S-PAC might improve virus removal, our objectives were to investigate the effect of pulverization of PAC particles on virus removal and the factors contributing to virus removal.

2. Materials and methods

2.1. Activated carbon

We tested 11 commercially available, thermally activated, normal PACs (N-PACs): 9 wood-based, 2 coconut-based, and 1 coal-based (Table 1). To prepare the S-PACs, we ground the N-PACs in a wet bead mill (Metawater Co., Ltd., Tokyo, Japan). We used both sets of materials to determine the effects of particle size on virus removal by adsorption. The PACs were dried in an oven at 105 °C and stored in a desiccator before use. They were then made into 5% slurries in Milli-Q water (Milli-Q Advantage, Millipore Corp., Billerica, MA, USA) and placed under vacuum to remove any air from the pores. The slurries were stored at 4 °C before dilution for use in the experiments. The particle size distributions were determined by laser scattering (LMS-30 Micron Sizer; Seishin Enterprise Co., Ltd., Tokyo, Japan). The surfaces of the N-PACs were observed by scanning transmission electron microscopy (SEM, JSM-7400F; JEOL Ltd., Tokyo, Japan).

* Corresponding author. Tel./fax: +81 11 706 7279.
E-mail address: taku-m@eng.hokudai.ac.jp (T. Matsushita).

1383-5866/$ - see front matter © 2013 Published by Elsevier B.V.
http://dx.doi.org/10.1016/j.seppur.2013.01.017

Table 1
Activated carbon used.

	Raw material	Median diameter (μm)		Key characteristics of S-PAC						
				Specific surface area[a] (m^2/g)	Element contents[b] (%)				Functional group[c]	
		S-PAC	N-PAC		C	O	N	S	Acidic	Basic
Wood-1	Wood	0.69	13.24	1145 ± 33	85.3 ± 0.6	7.05 ± 0.97	0.14 ± 0.01	0.10 ± 0.02	350 ± 9	790 ± 21
Wood-2	Wood	0.83	4.5	873 ± 39	80.0 ± 1.5	6.70 ± 0.51	0.25 ± 0.02	0.20 ± 0.02	193 ± 58	711 ± 139
Wood-3	Wood	1.49	NA	NA	NA	NA	NA	NA	NA	NA
Wood-4	Wood	0.66	NA	NA	84.6 ± 0.8	6.72 ± 0.11	0.15 ± 0.00	0.11 ± 0.03	NA	NA
Wood-5	Wood	2.79	NA	NA	NA	NA	NA	NA	NA	NA
Wood-6	Wood	1.38	NA	NA	NA	NA	NA	NA	NA	NA
Wood-7	Wood	2.20	NA	NA	NA	NA	NA	NA	NA	NA
Wood-8	Wood	0.93	11.46	1174 ± 14	81.9 ± 0.6	8.24 ± 0.48	0.20 ± 0.01	0.15 ± 0.02	351 ± 22	780 ± 56
Wood-9	Wood	1.65	0.6	NA	NA	NA	NA	NA	NA	NA
Coconut-1	Coconut shell	0.67	NA	NA	88.1 ± 0.5	5.95 ± 0.41	0.16 ± 0.02	0.11 ± 0.03	425 ± 34	329 ± 35
Coconut-2	Coconut shell	0.65	19.13	1215 ± 149	89.1 ± 0.2	5.30 ± 0.10	0.18 ± 0.04	0.06 ± 0.02	433 ± 16	582 ± 29
Coal-1	Coal	0.67	NA	NA	79.2 ± 0.3	10.62 ± 0.24	0.38 ± 0.00	0.55 ± 0.01	757 ± 36	366 ± 36
Determination coefficient (r^2) between logarithmic virus removal indicated in Fig. 2				0.38	0.01	0.06	0.06	0.06	0.08	0.10

NA – not applicable.
[a] Determined with BET.
[b] Measured with an elemental analyzer (Vario EL III, Elementar Analysensysteme GmbH, Hanau, Germany).
[c] Measured with Boehm titration [28,29].

2.2. Viruses

As model viruses we used two bacteriophages, Qβ (NBRC 20012) and MS2 (NBRC 20015), obtained from the Biological Resource Center (NBRC) of the National Institute of Technology and Evaluation (Chiba, Japan). The diameters of Qβ and MS2 are 23.5 ± 0.8 nm and 22.5 ± 1.0 nm, respectively [10]. The viruses were propagated for 22–24 h at 37 °C in *Escherichia coli* F^+ (NBRC 13965) obtained from NBRC. The cultures were centrifuged at 3000*g* for 10 min and then filtered through a 0.45-μm pore-size membrane (cellulose acetate; DISMIC-25cs; Toyo Roshi Kaisya, Ltd., Tokyo, Japan). The filtrate was purified twice in a centrifugal filter device (molecular weight cutoff: 100,000; Centriplus-100; Millipore Corp., Billerica, MA, USA) to prepare virus stock solution. Virus concentrations were measured by the plaque-forming unit (PFU) method according to the agar overlay method [11] using the bacterial host *E. coli* F^+. Average plaque counts of triplicate plates prepared from one sample gave the virus concentration.

2.3. Batch adsorption test

Milli-Q water was buffered with 424 μM $NaHCO_3$ to give the equivalent of 20 mg-$CaCO_3$/L of alkalinity (buffered Milli-Q water). The buffered Milli-Q water was supplemented with 0, 100, 200, 300, 400, or 500 μM $CaCl_2$. In a square beaker, 500 mL of solution was adjusted to pH 6.8 with HCl, and either Qβ or MS2 was added to give 10^6 PFU/mL. PAC was added at 20 mg/L and the suspension was continuously stirred at $G = 200\ s^{-1}$ with a jar tester. Samples were withdrawn at 0, 1, 2, 4, and 8 h and filtered through a membrane ($\phi = 0.2$ μm, PTFE; Toyo Roshi Kaisya) to remove the PAC particles. The virus concentration in the permeate was measured by the PFU method.

2.4. Electrophoretic mobility

All solutions were held for 1 day at 20 °C for the pH to stabilize. Just before measurement, each S-PAC or virus was suspended in the solution at ~20 mg/L or 10^9 PFU/mL, respectively. The electrophoretic mobility of S-PACs and viruses was measured with an electrophoretic light-scattering spectrophotometer (Zetasizer Nano ZS, 532 nm green laser; Malvern Instruments Ltd., Malvern, Worcestershire, UK) at 25 °C and at a 17° measurement angle.

2.5. Pore size distribution analyses of PACs

Pore size was analyzed by nitrogen gas adsorption at 77 K with an automated gas sorption analyzer (Autosorb-iQ-MP; Quantachrome Instruments, Boynton Beach, FL, USA). Pore size distributions were determined by a combination of two widely accepted models: the DFT model for the pore size distribution of micropores (<2 nm) and the BJH theory for the volumes of mesopores and macropores (>2 nm).

2.6. Virus hydrophobicity

Hydrophobicity was estimated by the bacterial adhesion to hydrocarbon (BATH) method [12]. Virus was added to 3 mL of buffered Milli-Q water at a final concentration of ~10^8 PFU/mL at pH 7.0. The solution was supplemented with 0.25 mL of solvent (*n*-hexadecane, *n*-octane, or *p*-xylene). The solution was intensely vortexed for 2 min, and then rested for 15 min at room temperature to allow the solvent and water to separate. The virus concentration in the water phase was measured by real-time PCR [13]. A decrease in virus concentration was used as a measure of the virus surface hydrophobicity [12].

3. Results and discussion

3.1. Comparison of virus removal between N-PACs and S-PACs

Virus removal increased with time even without PAC dosing (black circles), probably owing to spontaneous inactivation (Fig. 1). N-PACs (white circles) of wood-8 and coconut-2 showed the same result as the control. S-PACs of wood-8 and coconut-2 (gray circles) also showed the same result, even though their outer surface areas per unit mass were 12.3× and 29.4× those of the N-PACs, respectively. N-PAC of wood-1 removed some virus. In contrast, S-PAC of wood-1, with 19.2× the outer surface area of the N-PAC, caused a monotonic decrease in virus concentration with contact time, reaching a 4 log reduction after 8 h. Our result appears to disagree with that of Powell et al. [14], who reported

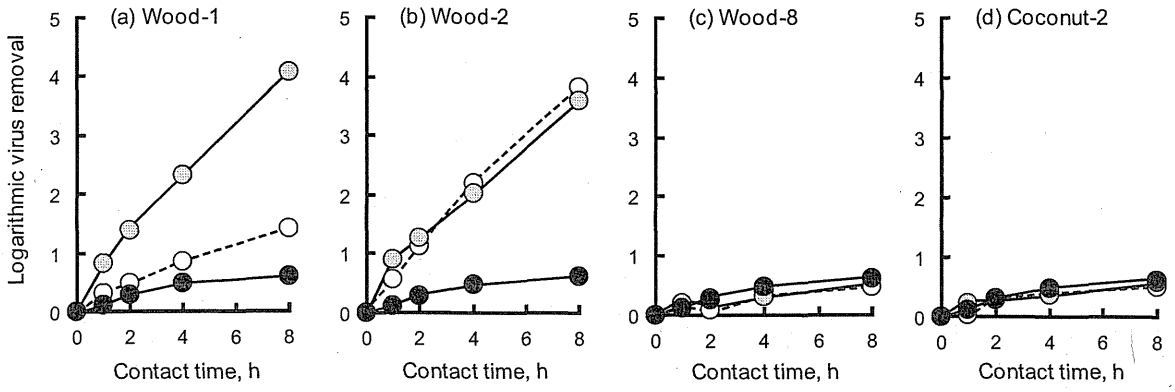

Fig. 1. Changes in virus (Qβ) removal with contact time (Ca^{2+} = 100 μM). Gray, white and black circles indicate SPAC, N-PAC and control, respectively.

that the adsorption of bacteriophage MS2 to a GAC reached equilibrium in 3 h. However, whereas they found that the amount of virus *adsorbed* had plateaued (>99% removal), we monitored the concentration of virus in the *liquid phase*, which might have decreased further even after 99% of the virus was adsorbed. N-PAC of wood-2 removed virus at the same extent as S-PAC of wood-1, possibly because the particle size of N-PAC of wood-2 was much smaller than those of other N-PACs. Virus removal with S-PAC of wood-2 was almost the same to that with the N-PAC, possibly because the N-PAC was small enough to remove the virus and its outer surface area was not so much increased with the pulverization (5.4×). The pulverization enhanced the adsorptive removal by the wood-1 PAC, but not by the wood-2, wood-8 and coconut-2 PACs. Overall, the effect of pulverization on virus removal might depend on the intrinsic characteristics of the PACs.

3.2. Effects of median diameter and PAC source on virus removal

We expected that finer PACs would remove more virus. However, different S-PACs with the same median diameter of ~0.7 μm showed very different removals of virus: wood-1 and wood-2 S-PACs achieved a removal of ~4 orders of magnitude (4 logs), whereas the other S-PACs achieved a removal of <2 logs (Fig. 2). Virus removal may be influenced by many factors such as raw material, specific surface area, element content, surface functional group, pore size distribution and surface charge. Nevertheless, as the capacity of the wood-based PACs varied widely from 0.5 to 4 logs, and a coconut-based PAC removed more virus than some wood-based PACs, the difference in virus removal seems to be due to more than the raw materials. The inherent characteristics of PAC listed in Table 1, i.e. specific surface area, element content and surface functional group, obviously had no relationship with the virus removal ($r^2 < 0.4$); other inherent factors most likely had influence on the adsorptive removal. To investigate the factors affecting the removal, we made a comparison in the following sections among two S-PACs that exhibited the highest virus removal (i.e. wood-1 and wood-2 S-PACs) and 2 S-PACs that had similar particle diameters to the superior S-PACs but exhibited the lowest virus removal (i.e. wood-8 and coconut-2 S-PACs).

3.3. Effect of surface charge of PACs on virus removal

When virus and S-PACs were dispersed in buffered Milli-Q water without Ca^{2+}, both particles were highly negatively charged, and the electrostatic repulsive force between them, measured as electrophoretic mobility, was high (Fig. 3). As the Ca^{2+} concentra-

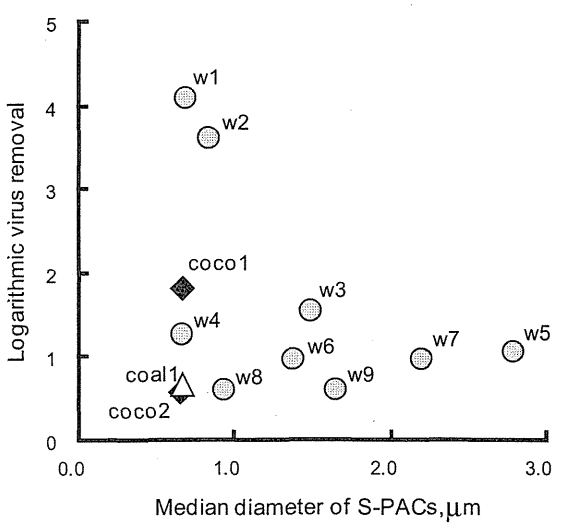

Fig. 2. Relationship between median diameter of S-PACs and virus removal (contact time = 8 h, Ca^{2+} = 100 μM). Circles, diamonds and triangle represent wood-, coconut- and coal-based SPACs. Logarithmic virus removals for wood-1, wood-2, wood-8 and coconut-2 S-PACs were averaged values of two experiments with too small deviations to see, while those for other S-PACs were obtained in one experiment.

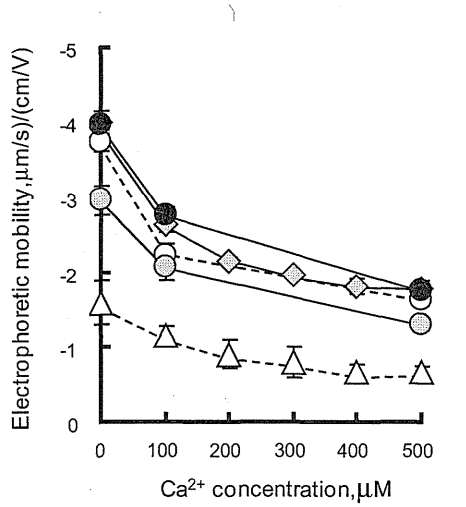

Fig. 3. Electrophoretic mobility of Qβ and S-PACs at different concentrations of Ca^{2+}. White, gray and black circles, gray diamonds and white triangles indicate wood-1, wood-2, wood-8, coconut-2 and Qβ, respectively. Error bars indicate SD of 10 measurements.

tion increased, the electrophoretic mobilities of both virus and S-PACs decreased. In general, an increase in ionic strength compresses the diffuse layer of ions surrounding a charged particle, decreasing the extent of the charge. This behavior has been seen before in viruses [15–18]. Our results support this.

The repulsion energy (V_R) of the electrical double layer between two closely spaced spheres is described as follows [19]:

$$V_R = 2\pi\varepsilon\zeta_1\zeta_2\frac{d_1d_2}{d_1+d_2}\exp(-\kappa h) \quad (1)$$

where ε is the permittivity of the medium, ζ_1 and ζ_2 are the zeta potentials of the spheres, d_1 and d_2 are the diameters of the spheres, and h is the minimum surface-to-surface separation between the spheres. κ is the Debye–Hückel reciprocal length:

$$\kappa = \sqrt{\frac{e^2\sum n_{i0}z_i^2}{\varepsilon kT}} \quad (2)$$

where e is the elementary charge, n_0 is the number concentration of ions in the bulk solution, z is the valency of the ion, k is the Boltzmann constant, and T is the absolute temperature. When virus and S-PAC were spaced 0.2 nm apart, as the Ca^{2+} concentration increased, the repulsion decreased (Fig. 4). Virus removal improved from 1–3 logs at 0 μM-Ca^{2+} to 3–6 logs at 500 μM-Ca^{2+}. Thus, virus removal was enhanced as the repulsion decreased. A higher ionic strength compresses the electrical double-layer of charged particles, reducing the electrostatic repulsion between like-charged particles and enabling the particles to move nearer to each other [17,21,22]. The adsorption of the virus onto the S-PAC was most likely hampered by the electrostatic repulsive force between them. Therefore, reducing the repulsion by increasing the ionic strength improved virus removal. One explanation is that the positive ions shield the negative charges on the surfaces of the adsorbate and the adsorbent, decreasing the net electrostatic repulsion between the particles [16,18,20,23]. Or Ca^{2+} may electrically adsorb to a negatively charged moiety of both adsorbate and adsorbent concurrently, forming a cation bridge to link the like-charged particles [18,23,24].

Fig. 5 shows the relationship between the virus removal and the electrical double layer repulsion energy. Virus removal tended to increase as the repulsive force decreased, but the removal performances were different among s-PACs. Wood-1 S-PAC exhibited superior virus removal across all repulsion energy range: the virus removal with wood-1 S-PAC was always greater than those with other S-PACs tested even in the range in which the repulsive force

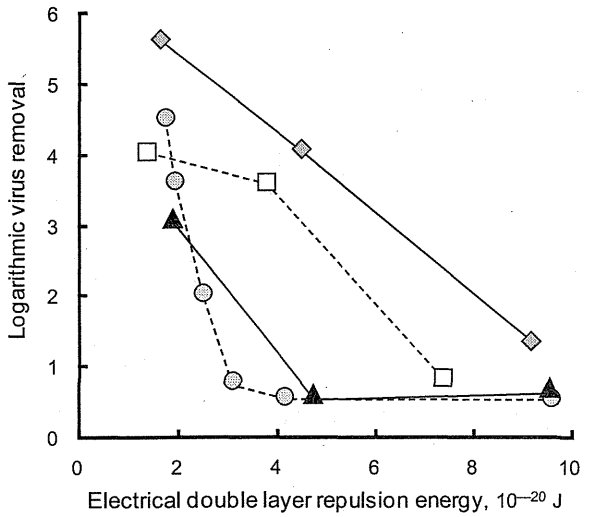

Fig. 5. Relationship between virus removal (Qβ, contact time = 8 h) and repulsion energy of electrical double layer (0.2 nm distance). Gray diamonds, white squares, black triangles and gray circles indicate wood-1, 2, 8 and coconut-2, respectively. Repulsion energy was controlled by Ca^{2+} concentration.

working between the virus and S-PAC particles was the same. These observations mean that the electrostatic repulsion can explain the extent of virus removal by each S-PAC under different ionic conditions, but not the difference between different types of PAC.

The logarithmic virus removals of wood-1 and wood-2 S-PACs linearly increased with decrease in the electrical double layer repulsion energy. In contrast, the virus removals of wood-8 and coconut-2 S-PACs did not change even when the repulsion energy decreased down from 10×10^{-20} to 3×10^{-20} J, but seem to increase drastically when the repulsion energy was smaller than 3×10^{-20} J. Possible reason for this observation is discussed in the following section.

3.4. Effect of pore size distribution of PACs on virus removal

SEM observations revealed that the wood-1 and wood-2 S-PACs, which could remove virus effectively, had a rough surface with many mesopores 20–50 nm in diameter (Photo 1). In contrast,

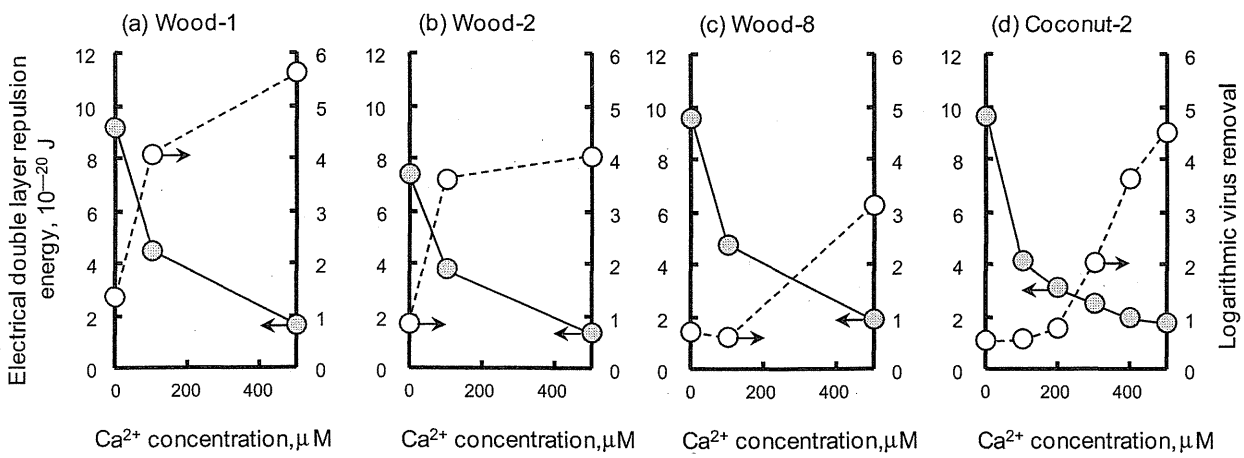

Fig. 4. Changes in repulsion energy of electrical double layer between the virus and S-PACs at 0.2 nm distance, and virus removal (Qβ, contact time = 8 h) with increase in Ca^{2+} concentration. Gray and white circles indicate the electrical double layer repulsion energy and the logarithmic virus removal, respectively.

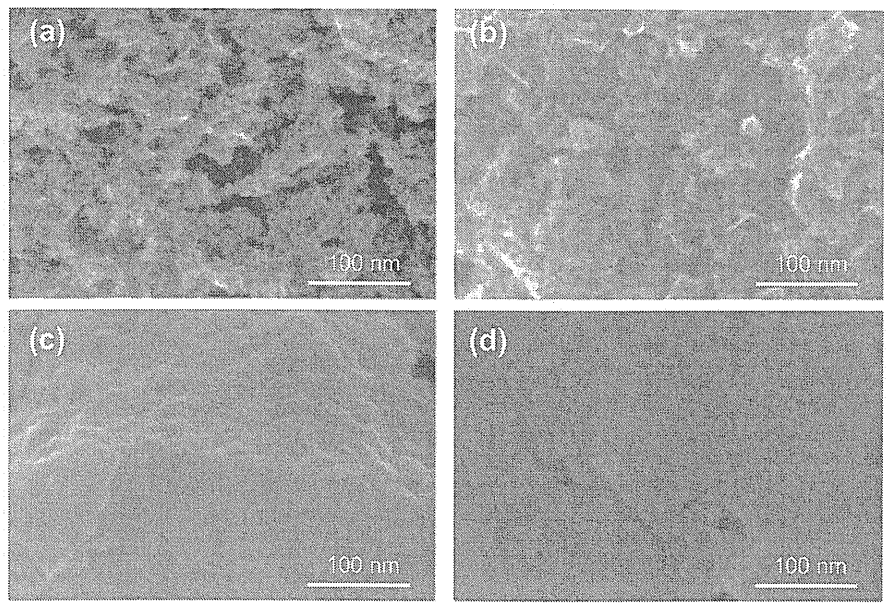

Photo 1. SEM images of S-PAC surfaces: (a) wood-1; (b) wood-2; (c) wood-8; and (d) coconut-2.

Table 2
Comparison in pore volume among S-PACs.

Pore diameter (nm)	Wood-1	Wood-2	Wood-8	Coconut-2
1–2	0.203	0.123	0.206	0.177
2–3	0.040	0.040	0.056	0.030
3–5	0.071	0.091	0.053	0.044
5–10	0.063	0.088	0.038	0.037
10–20	0.044	0.066	0.025	0.028
20–50	0.035	0.039	0.017	0.022

Table 3
Logarithmic removals of Qβ and MS2 with S-PACs (contact time = 8 h, Ca^{2+} = 100 μM).

	Wood-1	Wood-2
Qβ	4.1	3.6
MS2	3.0	2.9

the wood-8 and coconut-2 S-PACs, whose virus removal was poor, had a relatively smooth surface with no mesopores. With a diameter of ~23 nm, the virus cannot pass through pores smaller than this. The nearer the diameter of an adsorbate molecule is to the pore size of an adsorbent, the greater is the attraction [25]. Therefore, the wood-1 and wood-2 S-PACs, with pores 20–50 nm wide, offered good conditions for the virus to settle in, and so removed it effectively. This most likely contributed to the difference of behaviors of viruses in the relationship between the logarithmic virus removal and the electrical double layer repulsion energy indicated in Fig. 5: the wood-1 and wood-2 could easily capture the virus particles with many suitable pores for the virus particles to settle in even under the large repulsion energy that prevented the adsorption of the virus particles to the wood-8 and coconut-2 S-PACs. At this moment, the reason why the virus removals of wood-8 and coconut-2 S-PACs increased drastically with the decrease in the repulsion energy is not clear.

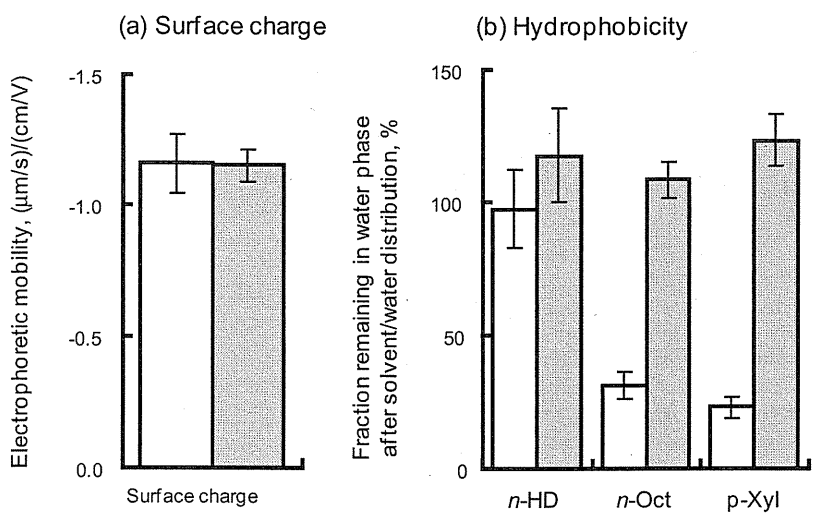

Fig. 6. Comparison of (a) surface charge and (b) hydrophobicity between Qβ and MS2. White and gray columns represent Qβ and MS2, respectively. *n*-HD, *n*-hexadecane; *n*-Oct, *n*-octanol; p-Xyl, p-xylene. Error bars in (a) and (b) indicate SD of 30 and 5 measurements, respectively.

Pore size measurements clearly show that the wood-1 and wood-2 S-PACs had larger pore volume at 20–50 nm than the wood-8 and coconut-2 S-PACs (Table 2); the pore volumes of the high-virus-adsorbable S-PACs were 1.8–2.0 times as much as the averaged pore volume of the low-virus-adsorbable S-PACs. These results agree well with the SEM observations, supporting the hypothesis that the pore size distribution of the S-PACs contributed greatly to virus removal.

3.5. Effect of hydrophobicity of virus on virus removal

The removal of bacteriophage MS2 was ~1 log less than that of Qβ by both wood-1 and wood-2 S-PACs (Table 3). Although the molecular size of an adsorbate controls accessibility to the pores of the activated carbon [26], the diameters of the Qβ and MS2 are almost the same (~23 nm), so this does not explain the difference in removal. Likewise, although the surface charges of viruses depend on the chemistry of their surface proteins, we found no difference in the surface charge between the two viruses (Fig. 6a). Instead, they differed in hydrophobicity (Fig. 6b): MS2 remained in the water phase of all solvent combinations tested, indicating that it has a hydrophilic surface. In contrast, Qβ largely transferred to the solvent phase when *n*-octane and *p*-xylene were used. This result indicates that the surface of Qβ is more hydrophobic than that of MS2, in agreement with a previous report [27]. Thus, the more hydrophobic the surface of the virus particles is, the greater the virus removal would be expected. As shown in Section 3.3, reducing the surface charge of the activated carbons improved virus removal. The reduction in the surface charge may provide more hydrophobic surface on the carbon apparently, because the reduction allows negatively charged adsorbates to move nearer to the graphite structure on the carbon. Adding to the reduction in the electrophoretic repulsive force, the apparent increase in hydrophobicity of the carbon surface most likely contributed to the high virus removal. Likewise, the hydrophobicity of the viruses contributed to the high removal: the virus having more hydrophobic surface was removed more greatly with the activated carbons.

4. Conclusions

(1) Electrophoretic repulsive force contributed greatly to virus removal: the smaller the repulsion between virus and PAC particles, the greater the virus removal.
(2) The pore size distribution of the PAC contributed greatly to virus removal: PACs with a large volume of pores 20–50 nm in diameter removed virus effectively.
(3) The hydrophobicity of the virus surface contributed greatly to virus removal: the more hydrophobic the surface, the greater the virus removal.
(4) To enhance adsorptive virus removal, activated carbons must have a less negative surface charge and a large volume of pores 20–50 nm wide.

Acknowledgments

Makoto Kobuke and Tomoko Aki made efforts for the experiments on the virus hydrophobicity and the surface functional group of the activated carbons, respectively. This research was supported in part by a Grant-in-Aid for the Encouragement of Young Scientists (2010) from the Ministry of Education, Culture, Sports, Science and Technology of Japan; a Grant-in-Aid (2010) from the Ministry of Health, Labor and Welfare of Japan; and a Kurita Water and Environment Foundation Research Grant (2009).

References

[1] C.P. Gerba, M.D. Sobsey, C. Wallis, J.L. Melnick, Adsorption of poliovirus onto activated carbon in wastewater, Environ. Sci. Technol. 9 (1975) 727–731.
[2] W.A. Hijnen, G.M.H. Suylen, J.A. Bahlman, A. Brouwer-Hanzens, G.J. Medema, GAC adsorption filters as barriers for viruses, bacteria and protozoan (oo)cysts in water treatment, Water Res. 44 (2010) 1224–1234.
[3] P.P. Oza, M. Chaudhuri, Removal of viruses from water by sorption on coal, Water Res. 9 (1973) 707–712.
[4] S.J. Randtke, V.L. Snoeyink, Evaluating GAC adsorptive capacity, J. AWWA 75 (1983) 406–413.
[5] I.N. Najm, V.L. Snoeyink, M.T. Suidan, C.H. Lee, Y. Richard, Effect of particle size and background natural organics on the adsorption efficiency of PAC, J. AWWA 82 (1990) 65–72.
[6] H. Sontheimer, J.C. Crittenden, R.S. Summers, Activated Carbon for Water Treatment, second ed., DVGW-Forschungsstelle, Karlsruhe, Germany, 1988.
[7] Y. Matsui, R. Murase, T. Sanogawa, N. Aoki, S. Mima, T. Inoue, T. Matsushita, Rapid adsorption pretreatment with submicron powdered activated carbon particles before microfiltration, Water Sci. Technol. 51 (6–7) (2005) 249–256.
[8] Y. Matsui, T. Sanogawa, N. Aoki, S. Mima, T. Matsushita, Evaluating submicron-sized activated carbon adsorption for microfiltration pretreatment, Water Sci. Technol.: Water Supply 6 (1) (2006) 149–155.
[9] Y. Matsui, N. Ando, H. Sasaki, T. Matsushita, K. Ohno, Branched pore kinetic model analysis of geosmin adsorption on super-powdered activated carbon, Water Res. 43 (2009) 3095–3103.
[10] N. Shirasaki, T. Matsushita, Y. Matsui, M. Kobuke, K. Ohno, Comparison of removal performance of two surrogates for pathogenic waterborne viruses, bacteriophage Qβ and MS2, in a coagulation–ceramic microfiltration system, J. Membrane Sci. 326 (2009) 564–571.
[11] M.H. Adams, Bacteriophages, Interscience, New York, NY, USA, 1959.
[12] M. Rosenberg, D. Gutnick, E. Rosenberg, Adherence of bacteria to hydrocarbons: a simple method for measuring cell-surface hydrophobicity, FEMS Microbiol. Lett. 9 (1980) 29–33.
[13] N. Shirasaki, T. Matsushita, Y. Matsui, A. Oshiba, K. Ohno, Estimation of norovirus removal performance in a coagulation-rapid sand filtration process by using recombinant norovirus VLPs, Water Res. 44 (2010) 1307–1316.
[14] T. Powell, G.M. Brion, M. Jagtoyen, F. Derbyshire, Investigating the effect of carbon shape on virus adsorption, Environ. Sci. Technol. 34 (2000) 2779–2783.
[15] S.L. Penrod, T.M. Olson, S.B. Grant, Whole particle microelectrophoresis for small viruses, J. Colloid Interface Sci. 173 (1995) 521–523.
[16] J.A. Redman, S.B. Grant, T.M. Olson, J.M. Adkins, J.L. Jackson, M.S. Castillo, W.A. Yanko, Physicochemical mechanisms responsible for the filtration and mobilization of a filamentous bacteriophage in quartz sand, Water Res. 33 (1999) 43–52.
[17] B. Yuan, M. Pham, T.H. Nguyen, Deposition kinetics of bacteriophage MS2 on a silica surface coated with natural organic matter in a radial stagnation point flow cell, Environ. Sci. Technol. 42 (2008) 7628–7633.
[18] S.E. Mylon, C.I. Rinciog, N. Schmidt, L. Gutierrez, G.C.L. Wong, T.H. Nguyen, Influence of salts and natural organic matter on the stability of bacteriophage MS2, Langmuir 26 (2010) 1035–1042.
[19] J. Gregory, Particles in Water: Properties and Processes, CRC Press, Boca Raton, FL, USA, 2006.
[20] J.C. Lance, C.P. Gerba, Effect of ionic composition of suspending solution on virus adsorption by a soil column, Appl. Environ. Microbiol. 47 (1984) 484–488.
[21] D.G. Jewett, T.A. Hilbert, B.E. Logan, R.G. Arnold, R.C. Bales, Bacterial transport in laboratory columns and filters: influence of ionic strength and pH on collision efficiency, Water Res. 29 (1995) 1673–1680.
[22] H. Cao, F.T.C. Tsai, K.A. Rusch, Impact of salinity on MS-2 sorption in saturated sand columns–fate and transport modeling, J. Environ. Eng. 135 (2009) 1041–1050.
[23] J. Zhuang, Y. Jin, Virus retention and transport through Al-oxide coated sand columns: effects of ionic strength and composition, J. Contaminant Hydrol. 60 (2003) 193–209.
[24] M. Pham, E.A. Mintz, T.H. Nguyen, Deposition kinetics of bacteriophage MS2 to natural organic matter: role of divalent cations, J. Colloid Interface Sci. 338 (2009) 1–9.
[25] R.J. Martin, Activated carbon product selection for water and wastewater treatment, Ind. Eng. Chem. Prod. Res. Dev. 19 (1980) 435–441.
[26] C. Moreno-Castilla, Adsorption of organic molecules from aqueous solutions on carbon materials, Carbon 42 (2004) 83–94.
[27] J. Langlet, F. Gaboriaud, J.F.L. Duval, C. Gantzer, Aggregation and surface properties of F-specific RNA phages: implication for membrane filtration processes, Water Res. 42 (2008) 2769–2777.
[28] H.P. Boehm, Some aspects of the surface-chemistry of carbon-blacks and other carbons, Carbon 32 (1994) 759–769.
[29] H.P. Boehm, Surface oxides on carbon and their analysis: a critical assessment, Carbon 40 (2002) 145–149.

WATER RESEARCH 47 (2013) 5819–5827

Available online at www.sciencedirect.com

SciVerse ScienceDirect

journal homepage: www.elsevier.com/locate/watres

Investigating norovirus removal by microfiltration, ultrafiltration, and precoagulation–microfiltration processes using recombinant norovirus virus-like particles and real-time immuno-PCR

Taku Matsushita, Nobutaka Shirasaki, Yuichi Tatsuki, Yoshihiko Matsui*

Graduate School of Engineering, Hokkaido University, N13W8, Sapporo 060-8628, Japan

ARTICLE INFO

Article history:
Received 22 May 2013
Received in revised form
2 July 2013
Accepted 2 July 2013
Available online 12 July 2013

Keywords:
Bacteriophage
Drinking water treatment
MS2
Norovirus
Qβ
Virus-like particles

ABSTRACT

The removal of microorganisms by drinking water treatment processes has been widely investigated in laboratory-scale experiments using artificially propagated microorganisms. However, this approach cannot be applied to norovirus removal, because this virus does not grow in cell or organ culture, and this fact has hampered our ability to investigate its behavior during drinking water treatment. To overcome this difficulty, our research group previously used recombinant norovirus virus-like particles (rNV-VLPs), which consist of an artificially expressed norovirus capsid protein, in laboratory-scale drinking water treatment experiments. However, the enzyme-linked immunosorbent assay (ELISA) method generally used to detect rNV-VLPs is not sensitive enough to evaluate high removal ratios such as those obtained by ultrafiltration (UF). We therefore developed and applied a real-time immuno-polymerase chain reaction (iPCR) assay for rNV-VLP quantification to investigate norovirus removal by microfiltration (MF), UF, and hybrid precoagulation–MF processes. The rNV-VLP detection limit with the developed iPCR assay was improved at least 1000-fold compared with ELISA. Whereas MF with a nominal pore size of 0.1 μm could not eliminate NV-VLPs, a 4-log reduction was achieved by UF with a molecular weight cutoff of 1 kDa. When MF was combined with precoagulation (≥10 μmol-Fe/L for ferric chloride; ≥20 μmol-Al/L for polyaluminum chloride; ≥40 μmol-Al/L for alum), the performance of the hybrid process in eliminating rNV-VLPs was greater than that achieved by the 1 kDa UF. For all processes, the removal ratios of the bacteriophages MS2 and Qβ were greater than the rNV-VLP removal ratios by 1–2 logs, so neither bacteriophage can be recommended as a possible conservative surrogate for predicting the behavior of native NV during these processes.

1. Introduction

Diarrhea is one of the greatest threats to human health worldwide, having been estimated to account for 15% of deaths in children younger than 5 years worldwide in 2008 (Black et al., 2010). Human caliciviruses, including *Norovirus* (NV), are recognized as a leading cause of diarrhea among persons of all ages (Patel et al., 2009). Because NV genome fragments have been detected in environmental waters (Westrell et al., 2006; Aw et al., 2009; Miura et al., 2009),

* *Corresponding author.* Tel./fax: +81 11 706 7279.
E-mail address: taku-m@eng.hokudai.ac.jp (T. Matsushita).
0043-1354/$ – see front matter © 2013 Elsevier Ltd. All rights reserved.
http://dx.doi.org/10.1016/j.watres.2013.07.004

outbreaks of epidemic diarrhea are possible if the raw water to be used for drinking water is contaminated with NV and the water is not adequately treated in the water treatment plant. In fact, Yang et al. (2011) reported that an outbreak of diarrhea due to norovirus in drinking water was caused by raw water contaminated with sewage being inadequately treated for particle removal and virus inactivation in a water treatment plant. Microorganisms can be removed from water by either disinfection or physical separation processes. Accordingly, it is of great importance from the viewpoint of public health to investigate ways to improve the processes used for the removal of NV during water treatment.

Virus-spiking experiments conducted in laboratory-scale treatment plants have been extensively used to investigate virus removal by drinking water treatment processes (Lénès et al., 2010; Bradley et al., 2011; Shi et al., 2012). Before such experiments can be performed, however, the virus must be artificially propagated. As NV does not grow in cell or organ culture and there is no small animal model for NV infection (Hutson et al., 2004), it is impossible to conduct removal experiments by spiking raw water with the artificially propagated virus for treatment by laboratory-scale plants. Accordingly, the removal of NV by drinking water treatment processes has been difficult to evaluate.

To overcome this difficulty, our research group previously investigated NV removal by using an artificially expressed NV capsid protein with a conventional drinking water treatment process consisting of coagulation, sedimentation, and rapid sand filtration (Shirasaki et al., 2010). The NV capsid protein spontaneously self-assembles into virus-like particles (VLPs) when expressed in insect cells infected with a recombinant baculovirus containing the gene encoding the capsid protein (Jiang et al., 1992). Because the recombinant NV VLPs (rNV-VLPs) are morphologically and antigenically the same as native NV particles, rNV-VLPs are expected to behave similarly to native NV during treatment processes. In what to our knowledge was the first attempt to apply rNV-VLPs to evaluate NV removal by drinking water treatment processes, our research group successfully used rNV-VLPs to evaluate NV removal by the conventional drinking water treatment process described above (Shirasaki et al., 2010).

Viruses are continuously and globally monitored in environmental waters. In most cases, the virus concentration is determined either by culturing, where it is reported as the number of plaque-forming units (PFUs), or by polymerase chain reaction (PCR) analysis. Because no culture method has been developed for NV, NV concentrations can be determined only by the latter method. However, rNV-VLPs contain no genomic material, precluding quantification by PCR. In addition to the PCR method, the enzyme-linked immunosorbent assay (ELISA) method has been used for NV quantification; for example, this method has been used with stool samples for the clinical diagnosis of viral infection with good results (Richards et al., 2003). However, ELISA is less sensitive than real-time PCR (Richards et al., 2003; de Bruin et al., 2006). Previously, we used a commercially available ELISA kit for NV to quantify the NV removal performance of the conventional drinking water treatment process (Shirasaki et al., 2010). The quantification was successful because the rNV-VLP concentrations after treatment were relatively high (i.e., the removal ratio was relatively low). However, after filtration through tight membranes with very small pore sizes, smaller rNV-VLP concentrations are expected. The ELISA quantification limit may thus be too poor for this method to be useful for evaluating rNV-VLP concentrations after membrane filtration processes. Thus, this limitation will hamper the use of the ELISA method for the evaluation of NV removal by such processes.

An immuno-PCR (iPCR) assay (Sano et al., 1992) can be used to obtain enhanced sensitivity for the detection and quantification compared with that of the ELISA method. An iPCR assay is an antibody-based immunoassay that uses nucleic acid amplification techniques for signal generation instead of the enzymatic reaction used in the conventional ELISA (Fig. 1). As a result, the sensitivity of the method is dramatically enhanced compared to that of ELISA. The iPCR assay has been applied mainly to the diagnosis of many different kinds of viruses (Maia et al., 1995; Mweene et al., 1996; Constantine et al., 2004; Adler et al., 2005). In the present study, we developed and applied an iPCR assay for the quantification of rNV-VLPs; we then used rNV-VLPs together with the iPCR method to evaluate NV removal by microfiltration (MF), ultrafiltration (UF), and precoagulation–MF processes. This study represents the first time an iPCR assay has been applied to the evaluation of microorganism removal by drinking water treatment processes.

2. Materials and methods

2.1. rNV-VLP and bacteriophages

The rNV-VLPs were prepared by a baculovirus–silkworm expression system, as in our previous study (Shirasaki et al., 2010). Briefly, subgenomic cDNA fragments of the NV genome (Chiba virus, AB042808, GI/4, Chiba407/1987/JP) were artificially synthesized. The fragments contained the entire second and third open reading frames and the 3′-UTR (untranslated region) of the NV genome. The cDNA was subcloned into a baculovirus transfer vector, and then the vector was transfected into silkworm cells. The expressed rNV-VLPs were separated from the cell lysate by centrifugation and dialysis. The diameter of the rNV-VLPs was 35.7 ± 3.2 nm (Shirasaki et al., 2010), which roughly corresponds to the particle diameter (approximately 38 nm) previously reported for native NV (Someya et al., 2000). The rNV-VLPs were quantified by an iPCR assay as described in Section 2.2.

Two bacteriophages, Qβ (NBRC 20012) and MS2 (NBRC 102619), were obtained from the National Institute of Technology and Evaluation (NITE) Biological Resource Center (NBRC, Chiba, Japan) for use as model viruses. The diameters of Qβ and MS2 are 23–24 nm (Shirasaki et al., 2009). *Escherichia coli* F^+ (NBRC 13965) obtained from NBRC was propagated for 3 h at 37 °C according to the supplier's instructions to prepare an *E. coli* F^+ suspension. The bacteriophages were then propagated for 22–24 h at 37 °C in the *E. coli* F^+ suspension. The respective bacteriophage cultures were centrifuged (2000 × *g*, 10 min) and then filtered through a membrane filter with a pore size of 0.45 μm (cellulose acetate; DISMIC-25cs; Toyo Roshi Kaisya, Tokyo, Japan). The filtrate was purified by using a centrifugal filter device (molecular weight cutoff [MWCO],

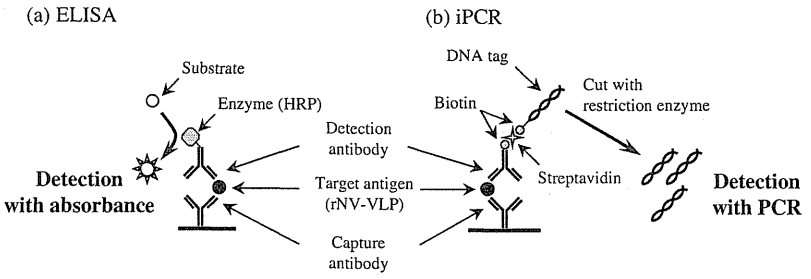

Fig. 1 – Schematic comparison of the ELISA and iPCR methods.

100,000; regenerated cellulose, Amicon Ultra-15; Millipore, Billerica, MA, USA) to prepare the virus stock solution. The bacteriophages were individually quantified by the real-time RT-PCR method with a TaqMan probe and primers (Shirasaki et al., 2009) in an Applied Biosystems 7300 Real-Time PCR System (Applied Biosystems Japan Ltd., Tokyo, Japan).

2.2. iPCR and ELISA for rNV-VLP quantification

An iPCR assay was used to quantify the rNV-VLPs. Ten types of monoclonal antibodies to rNV-VLPs were obtained by orally feeding rNV-VLPs to mice (Japan Lamb Ltd., Fukuyama, Japan), and the two most sensitive antibodies out of the 10 antibodies obtained were used for the iPCR assay. One antibody (IgM) was immobilized in the wells of 8-well microplates (TopYield modules, Nalge Nunc International, Penfield, NY, USA) and used to capture the rNV-VLPs, and the other (IgG) was biotinylated and then used for detection. An aliquot of 50 μL of either a sample or a river water (as a negative control) was placed in each well of the 8-well microplates and left at 37 °C for 90 min so as to allow the rNV-VLPs to be captured by the immobilized antibody. The sample solutions were discarded, and then the wells were washed six times with 150 μL of phosphate-buffered saline solution with Tween 20 (PBST). Next, the wells were supplemented with 50 μL of the biotinylated detection antibody (1 μg/mL) in a stabilizing reagent (Immuno Shot Reagent 2, Cosmo Bio Co. Ltd., Tokyo, Japan), and then kept at 37 °C for 90 min so as to allow the detection antibodies to adsorb onto the captured rNV-VLPs. The solutions were discarded, and the wells were washed six times with 150 μL of PBST. The wells were then supplemented with 50 μL of streptavidin (0.1 μg/mL) in a blocking agent solution (1%, Block Ace, DS Pharma Biomedical Co., Ltd., Suita, Japan), and then kept at 37 °C for 60 min so as to allow the avidin to adsorb to the biotin. The solutions were discarded, and the wells were washed six times with 150 μL of PBST. The wells were supplemented with 50 μL of biotinylated DNA tag (480 bp, CareTIS, Co., Ltd., Mobara, Japan), and then kept at 37 °C for 60 min so as to allow the DNA tag to adsorb to the immobilized rNV-VLPs via biotin–avidin interactions. The solutions were discarded, and the wells were washed six times with 150 μL of PBST. The wells were supplemented with 50 μL of *Eco*RI (restriction enzyme) (Promega KK, Tokyo, Japan) so as to allow a portion of the DNA tag to be released from the immobilized antibody–antigen complex. A portion (4 μL) of the solution was subjected to RT-PCR to measure the rNV-VLP concentration by the SYBR Green method (forward primer, 5′-GAAGGAGCGAGTGACTGAG-3′; reverse primer, 5′-CGTAATTACTTAGCCGGTTG-3′) in a Real-Time PCR System following the manufacturer's instructions.

So that we could compare the sensitivity of iPCR for rNV-VLPs with that of ELISA, ELISA was performed with the same two antibodies described above. IgM was immobilized on 8-well microplates to capture the rNV-VLPs, and IgG was conjugated with horseradish peroxidase (HRP) and then used for detection. An aliquot of 50 μL of either a sample or a river water (as a negative control) was placed into each well of the 8-well microplates and left for 90 min at room temperature so as to allow the rNV-VLPs to be captured by the immobilized antibody. The sample solutions were discarded, and the wells were washed six times with 150 μL of PBST. The wells were supplemented with 50 μL of the HRP-conjugated detection antibody (final concentration, 2 μg/mL) in the blocking solution and then kept for 90 min at room temperature so as to allow the detection antibodies to adsorb to the captured rNV-VLPs. The solutions were discarded, and the wells were washed six times with 150 μL of PBST. The wells were supplemented with 50 μL of 3,3′,5,5′-tetramethylbenzidine and kept for 30 min at room temperature to allow the 3,3′,5,5′-tetramethylbenzidine to react with the HRP. After the addition of 50 μL of diluted sulfuric acid (0.3 mol/L) to the wells to terminate the reaction, optical densities at wavelengths of 450 nm and 630 nm in the 8-well microplate were measured with a microplate reader (MTP-300, Corona Electric Co., Ltd., Ibaraki, Japan). Both iPCR and ELISA were performed with two wells for each sample.

2.3. Membranes

For UF membranes, we used 47-mm discs made of regenerated cellulose (RC) (Ultracel, Millipore) having different nominal MWCOs of 1, 10, and 100 kDa. Direct filtration experiments with the UF membranes were conducted in a stirred ultrafiltration cell (Model 8050, Millipore) under a constant pressure mode of 500 kPa provided by pressurized nitrogen gas.

We used three types of organic MF membranes and one type of inorganic MF membrane. The organic MF membranes were 45.5-mm discs with a nominal pore size of 0.1 μm composed of polyvinylidene difluoride (PVDF) (hydrophilic Durapore, Millipore), polytetrafluoroethylene (PTFE) (Omnipore, Millipore), or a mixture of cellulose acetate and cellulose

nitrate (MC) (MF-Millipore, Millipore). Direct filtration experiments with an aspirator (EYELA A-1000S, Tokyo Rikakikai Co., LTD., Tokyo, Japan) were performed with the organic MF membranes. The inorganic MF membrane was a monolithic ceramic membrane (55-channel tubular; nominal pore size, 0.1 μm; effective filtration area, 0.043 m^2; membrane diameter, 0.03 m; membrane length, 0.1 m; NGK Insulators, Ltd., Nagoya, Japan), and it was mainly used in the hybrid precoagulation–MF process. The ceramic MF membrane was installed in a stainless steel casing.

2.4. Direct filtration experiments

To prepare raw water for the experiments, river water from the Toyohira River (Sapporo, Japan; turbidity, 1.3 NTU; dissolved organic carbon [DOC], 0.6 mg/L; OD_{260}, 0.02 cm^{-1}) was concomitantly spiked with rNV-VLPs (10^{10} VLPs/mL), Qβ (10^8 PFU/mL), and MS2 (10^8 PFU/mL), and the pH of the virus-spiked river water was adjusted to 6.8 with HCl. Fifty milliliters of the raw water was directly filtered using either a stirred ultrafiltration cell or an aspirator. The first 10 mL of the filtrate was discarded, and then the rest was stored for quantification of the rNV-VLPs and the bacteriophages. All direct filtration experiments were conducted three times.

2.5. Precoagulation–MF experiments

For the precoagulation–MF experiments, a small inline-coagulation system was used (Fig. 2). The virus-spiked river water was fed into the system at a constant flow rate (58 mL/min) by a peristaltic pump. HCl was added by another peristaltic pump (1 mL/min) before the first in-line static mixer (N40-172, Noritake Co., Ltd., Nagoya, Japan, hydraulic retention time; 1.8 s), with the dose being regulated so as to maintain the pH of the MF permeate at 6.8. When ferric chloride was used as the coagulant, additional experiments were performed at pH 5.8 and 6.3 because the optimum pH for ferric chloride is generally lower than that for aluminum coagulants (Pontius, 1990). Coagulant (polyaluminum chloride [PACl], alum, or ferric chloride) was injected by a peristaltic pump (1 mL/min) after the first in-line static mixer and before the second at various dosing rates (0, 10, 20, or 40 μmol-Al or -Fe/L). After mixing in the second static mixer (hydraulic retention time, 1.8 s), the water was fed into the monolithic ceramic MF module in dead-end mode. The filtration lasted for 30 min without any backwash. Virus concentrations in the raw water tank and in the MF permeate were measured every 5 min. All precoagulation–MF experiments were conducted three times.

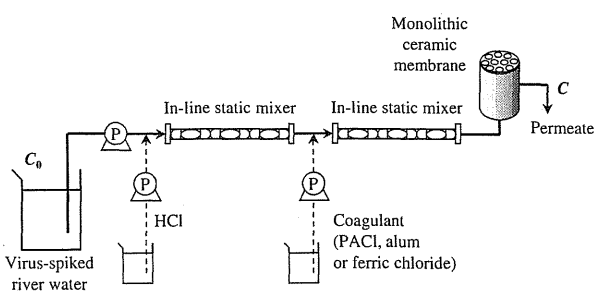

Fig. 2 – Experimental setup of the precoagulation–microfiltration system.

2.6. Precoated MF experiments

To investigate whether aluminum flocs retained on the membrane surface affected virus removal, direct filtration experiments were conducted with the ceramic MF membrane precoated with aluminum flocs as follows. Aluminum flocs were accumulated on the membrane surface by continuously feeding unspiked river water (without any virus) into the precoagulation–MF system (PACl, 20 μmol-Al/L). After a predetermined filtration time (30, 60, or 120 min), the raw water was switched to virus-spiked river water, and then direct filtration experiments were conducted on the precoated membranes without any coagulant dosing for the next 30 min. Virus concentrations in the raw water tank and the MF permeate were measured every 5 min.

3. Results and discussion

3.1. Quantification of rNV-VLPs by the iPCR assay

We first examined the rNV-VLP calibration curve obtained with the ELISA method (Fig. 3a). The rNV-VLP concentration was linearly correlated with logarithmic absorbance in the range from 10^8 to 10^{10} VLPs/mL, whereas for rNV-VLP concentrations equal to or smaller than 10^8 VLPs/mL, the observed absorbance was constant and almost the same as that of the negative control (Fig. 3a). This results indicates that with the ELISA kit it is possible to quantify rNV-VLP concentrations of $>10^8$ VLPs/mL. This result roughly corresponds to that obtained by using a commercially available ELISA kit for NV (Shirasaki et al., 2010).

The RT-PCR standard curve for the DNA tag used in the iPCR protocol showed a correlation of 1.00 in the range of 10^3 and 10^9 copies/mL (data not shown), indicating that the SYBR Green RT-PCR of the DNA tag was properly conducted. In the iPCR assay developed in the present study, the DNA tag of even the negative control, which contained no rNV-VLPs, was amplified; and a positive threshold cycle (Ct) value was observed (dashed line in Fig. 3b), as has been generally reported by previous studies, probably because of non-specific adsorption of the biotinylated DNA tag (McKie et al., 2002; Adler et al., 2008) or contamination of the reagents or equipment with the DNA tag (McKie et al., 2002). The elevated fluorescence exhibited by the negative control limited the sensitivity of the iPCR assay; but in the range from 10^5 to 10^9 VLPs/mL, the Ct values observed were smaller than that obtained for the negative control. This result means that the iPCR assay could detect rNV-VLPs in that concentration range. In that range, the rNV-VLP concentration was linearly correlated with the Ct value ($r^2 = 0.99$). These results showed that the iPCR method can quantify rNV-VLP concentrations of $\geq 10^5$ VLPs/mL. Thus, the detection limit of the iPCR assay for rNV-VLPs was improved at least 1000-fold compared with that of the ELISA method. Most studies using an iPCR assay have reported a 100- to 1000-fold improvement in the detection

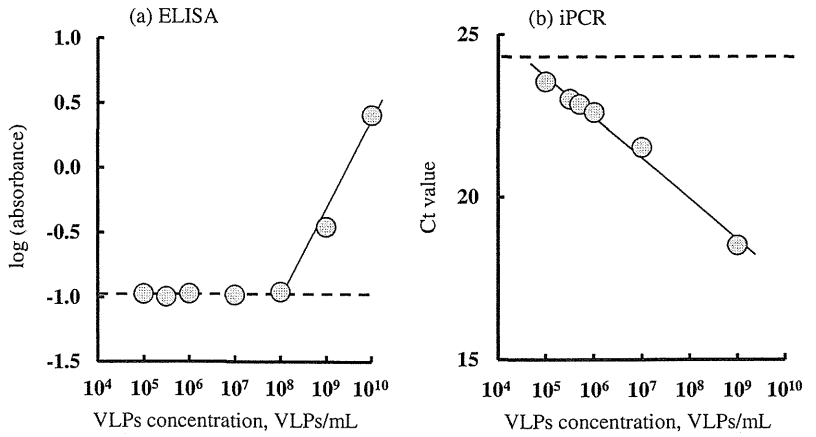

Fig. 3 – rNV-VLP calibration curves obtained with (a) ELISA and (b) iPCR. The dashed lines represent the results obtained with the negative control. Ct value = threshold cycle value.

limit (Adler et al., 2008), in agreement with the result obtained in this study. In our iPCR assay, an aliquot of 50 μL of test sample was added to each well for measurement. Accordingly, the detection limit for rNV-VLPs (10^5 VLPs/mL) is equivalent to 5×10^3 VLPs/well. Tian and Mandrell (2006) developed an iPCR assay for rNV-VLPs and reported a detection limit of 10^2 VLPs/well, which is smaller than our limit, but Adler et al. (2008), who reviewed many iPCR reports, found that the typical detection limit for proteins was approximately 10^3 molecules/well, which is of the same order of magnitude as the detection limit obtained by the present study.

Because the bacteriophages Qβ and MS2 were added to the raw water along with the rNV-VLPs in the membrane filtration experiments conducted in the present study, so that their removal rates could be compared with the rNV-VLP removal rate, the water samples contained not only rNV-VLPs but also the bacteriophages. Accordingly, before performing the membrane filtration experiments, we investigated cross-reactions between the antibodies and the bacteriophages. The river water used in the membrane filtration experiments was first supplemented with both Qβ and MS2 at 10^8 PFU/mL, and then the rNV-VLPs were serially diluted with the bacteriophage-spiked river water to make 10^5–10^9 VLPs/mL of rNV-VLP solution (i.e., the concentrations of the bacteriophages were the same in all diluted rNV-VLP solutions). The iPCR assays performed on the bacteriophage-containing rNV-VLP solutions and on rNV-VLP solutions diluted with river water without bacteriophages revealed no differences between the solutions (data not shown), the indication being that iPCR as employed could quantify rNV-VLPs without cross-reactions occurring, even when the concentration of bacteriophages was high.

3.2. *Removal of rNV-VLPs by the direct MF or UF processes*

We compared virus removal by direct UF or MF (Fig. 4). Irrespective of the composition of the MF membrane, the removal ratios of rNV-VLPs and bacteriophages by the MF membranes were smaller than 0.6 log. Therefore, the MF membranes could not effectively remove viruses from the raw water, because the diameters of the rNV-VLPs and the two bacteriophages (36 and 23–24 nm, respectively) were smaller than the MF membrane pore size (nominally 100 nm). Our results agree with those of a previous study in which the retention of bacteriophage Qβ by MF membranes with a nominal pore size larger than 20 nm was very low (Urase et al., 1996). Herath et al. (1999) also reported that removal ratios of Qβ and MS2 by a MF membrane having a nominal pore size of 50 nm at around pH 7 were 20–30% (i.e., 0.1–0.2 log), values that roughly agree with ours.

The removal ratios of rNV-VLPs were slightly improved with UF membranes having MWCOs of 10 and 100 kDa compared with the MF membranes, but they were still small (approximately 1.5 log). Because an rNV-VLP is composed of 90 capsid protein dimers (Prasad et al., 1994) and each capsid protein has a molecular weight of 58 kDa (Jiang et al., 1992;

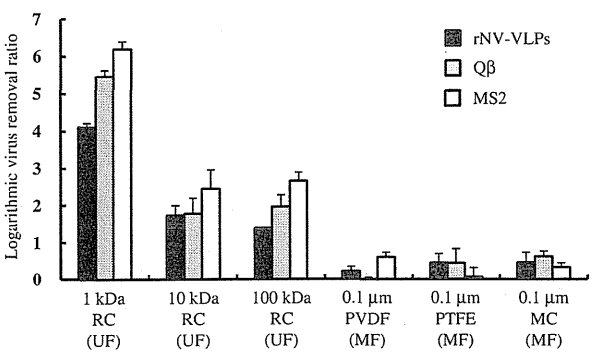

Fig. 4 – Virus removal by different ultrafiltration (UF) or microfiltration (MF) membranes: RC, regenerated cellulose; PVDF, polyvinylidene difluoride; PTFE, polytetrafluoroethylene; MC, mixture of cellulose acetate and cellulose nitrate. The columns and error bars represent the averages and standard deviations, respectively, of three runs.

Prasad et al., 1994), the molecular weight of an rNV-VLP is calculated to be approximately 10,000 kDa. The molecular weight of each rNV-VLP was therefore 1000–10,000 times the MWCOs of these two UF membranes. Accordingly, we expected high retention on these UF membranes. However, in terms of their pore geometry, UF membranes generally consist of an interconnected three-dimensional network of channels of non-uniform size and shape (Jeon et al., 2008). Thus, each UF membrane is characterized by a pore size distribution, and the nominal MWCO guarantees only a 90% rejection rate (i.e., a 1-log reduction) of compounds with that molecular weight. The UF membranes with MWCOs of 10 and 100 kDa probably had a wide pore-size distribution range over their MWCOs, with the result that a reduction of only 1.5 log was observed for the rNV-VLPs. In contrast, the rNV-VLPs were effectively removed (4-log removal) by the UF membrane with a MWCO of 1 kDa. The pore size distribution of this UF membrane likely included a region of smaller pore sizes than the distributions of the UF membranes with MWCOs of 10 and 100 kDa. As a result, the 1 kDa UF membrane could effectively retain the rNV-VLP particles.

The removal ratios of the bacteriophages by the UF membranes tended to be similar to those of the rNV-VLPs: the removal ratios by UF membranes with MWCOs of 10 and 100 kDa were almost the same (1.8–2.7 log), and those by the UF membrane with a MWCO of 1 kDa were much larger (5.5–6.2 log) than those by the UF membranes with MWCOs of 10 and 100 kDa. The removal ratios of the bacteriophages were always greater than those of the rNV-VLPs, even though the bacteriophage diameters were smaller than the rNV-VLP diameter. Important factors affecting rejection of viruses by membranes include electrostatic and hydrophobic interactions in addition to the ratio of the membrane pore diameter to the virus diameter (Madaeni et al., 1995; Langlet et al., 2009). Virus particles electrostatically adsorb to filter media when the filter media and the virus particles have unlike charges. When they have like charges, the virus particles are repulsed by the filter media, and then they are able to pass through the media (Dowd et al., 1998). The UF membranes used in the present study were negatively charged (Kwon et al., 2008), and both the rNV-VLPs and the bacteriophages were also negatively charged at pH 6.8 (Shirasaki et al., 2010). Thus, it is unlikely that electrostatic adsorption caused retention of the virus particles. Instead, hydrophobic interaction may have contributed to the virus retention; hydrophobic viruses tend to be more difficult for hydrophilic membranes to remove than hydrophilic viruses (Langlet et al., 2009). Qβ is more hydrophobic than MS2 (Langlet et al., 2008; Matsushita et al., 2013), and the UF membranes used in the present study were hydrophilic. Accordingly, Qβ was most likely removed by the UF membranes to a lesser extent than MS2 because of its greater hydrophobicity. The rNV-VLPs may be more hydrophobic than either bacteriophage.

3.3. *Removal of rNV-VLPs by the hybrid precoagulation–MF process*

Fig. 5 shows the removal ratios of rNV-VLPs by in-line coagulation followed by a ceramic MF. When the ceramic MF was used without precoagulation (0 μmol/L of coagulant), no rNV-

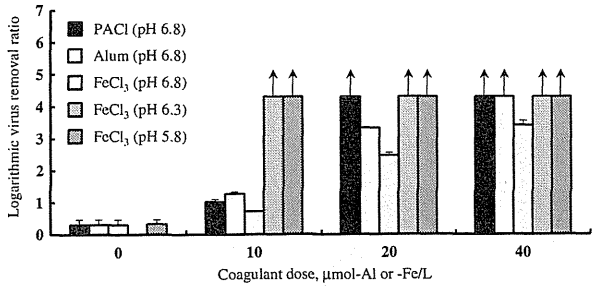

Fig. 5 – rNV-VLP removal by in-line coagulation followed by a ceramic microfiltration membrane having 0.1 μm diameter pores. The columns and error bars represent averages and standard deviations, respectively, of three runs. The arrows indicate virus concentrations below the quantification limit.

VLP removal was observed (<0.3 log), as with the organic MF membranes. When the precoagulation process was used with 10 μmol-Al/L of PACl coagulant prior to the MF process (black column), the removal was slightly improved, up to approximately 1.0 log. When the PACl dose was increased to ≥20 μmol-Al/L, the removal was dramatically improved, up to ≥4.3 log. The virus removal observed in the present study was most likely caused by sweep coagulation, because charge neutralization with aluminum salts generally occurs at low aluminum concentrations, usually on the order of a few micromoles per liter at a pH around neutral (Gregory, 2006). Positively charged sweep aluminum flocs (amorphous aluminum hydroxide, $Al(OH)_3$) (Davis and Leckie, 1978) were efficiently formed with a PACl dose of ≥20 μmol-Al/L, and rNV-VLPs were effectively incorporated into the sweep flocs. Because the size of the sweep flocs with incorporated rNV-VLPs was greater than the membrane pore size, the rNV-VLPs were effectively rejected by the membrane along with the sweep flocs. Additionally, rNV-VLPs that did not become enmeshed in the sweep flocs during the precoagulation step were probably adsorbed to the sweep flocs that were retained as precipitate on the MF membrane surface when the rNV-VLPs encountered the precipitate. According to Shirasaki et al. (2010), coagulation–rapid sand filtration fails to remove rNV-VLPs with a PACl dose of ≤20 μmol-Al/L; rather, a PACl dose of ≥40 μmol-Al/L is required for a reduction of approximately 3 logs. The ceramic MF process was superior to the rapid sand filtration process for solid/liquid separation after coagulation in terms of the coagulant dose required and the removal ratio of the rNV-VLPs. Moreover, the rNV-VLP removal performance of precoagulation with PACl doses of ≥20 μmol-Al/L followed by the ceramic MF process was higher than the performance of direct UF by the membrane with a MWCO of 1 kDa.

When the experiments were conducted with alum coagulant (white columns), rNV-VLPs were efficiently removed by the hybrid system, but the removal ratios were slightly smaller than those obtained with PACl as the coagulant. During the coagulation process, many aluminum species are generated by hydrolysis of aluminum coagulants. Among

them, the polycationic species Al_{13} ($[AlO_4Al_{12}(OH)_{24}(H_2O)_{12}]^{7+}$) is believed to be the most active species responsible for coagulation (Bottero et al., 1982; Parthasarathy and Buffle, 1985). Virus removal by PACl may have been enhanced compared to that by alum, because PACl contains more preformed Al_{13} than alum (Van Benschoten and Edzwald, 1990; Gregory, 2006).

When the experiments were conducted with ferric chloride coagulant at pH 6.8 (light gray columns), the rNV-VLP removal ratios were smaller than those with the aluminum coagulants. However, when the coagulation pH was lowered to 6.3 or 5.8, rNV-VLP removal was dramatically improved. The reported optimal pH range of the coagulation–sedimentation process with ferric chloride for DOC removal is less than 6.0 (Abbaszadegan et al., 2007). In the same manner, the removal of rNV-VLPs was improved when the pH was reduced from neutral to acidic. At pH 6.3 and 5.8, removal ratios ≥4.3 logs were observed even with 10 μmol-Fe/L of coagulant. These removal ratios were greater than those with PACl or alum. Chang et al. (1958) also reported greater removal of Coxsackie viruses and a bacteriophage with ferric chloride than with alum by a coagulation–sedimentation process at pH 6.2.

Similar to the rNV-VLPs, the bacteriophages were effectively removed by the MF membrane after precoagulation with PACl (Fig. 6), but the removal ratios of the bacteriophages were greater than those of the rNV-VLPs. Different from direct filtration, with a precoagulation–MF system, hydrophobic interaction between the virus particles and the membrane is probably not an important factor in determining virus removal ratios. Instead, interaction between the virus particles and the hydrolyzing aluminum species likely played an important role. Shirasaki et al. (2010) reported that the removal ratios of rNV-VLPs by a coagulation–sedimentation process were smaller than those of the bacteriophages Qβ and MS2 because of differences in affinity with the hydrolyzing aluminum species, possibly originating from differences in the hydrophobicity of the viruses. The same phenomenon probably occurred during the precoagulation process employed in the present study and thus can explain the differences in the rNV-VLP and bacteriophage removal ratios by the hybrid precoagulation–MF process. Additionally, the extent of electrostatic adsorption of the virus particles onto positively charged aluminum flocs retained on the membrane surface as precipitates also probably affected the removal performance. The rNV-VLPs are less negative than the bacteriophages (Shirasaki et al., 2010). Accordingly, the extent of electrostatic adsorption of rNV-VLPs to the aluminum precipitates was likely smaller compared with that of the bacteriophages, because the magnitude of the electrostatic attractive force between two unlike charges is proportional to the scalar product of the magnitudes of the charges. This difference probably also contributed to the differences in the virus removal performance between rNV-VLPs and the bacteriophages observed in the present study. Even without precoagulation, the ceramic MF membrane precoated with aluminum flocs (Fig. 7) was able to remove viruses, and this result clearly implies that the virus particles were adsorbed onto the retained aluminum precipitates. Overall, in terms of the contribution to the virus removal, the affinity of the virus particles for the hydrolyzing aluminum species and the aluminum precipitates most likely had a greater impact than hydrophobic interactions between the virus particles and the membrane. As a result, the removal ratios of the bacteriophages were always greater than those of the rNV-VLPs. Because of their greater removal ratios, neither Qβ nor MS2 can act as a conservative surrogate of NV in a hybrid precoagulation–MF system. Even taking into account the high removal ratios of the bacteriophages in a direct UF or precoagulation–MF hybrid system, the estimated removal of NV was 1–2 logs smaller than those of the bacteriophages.

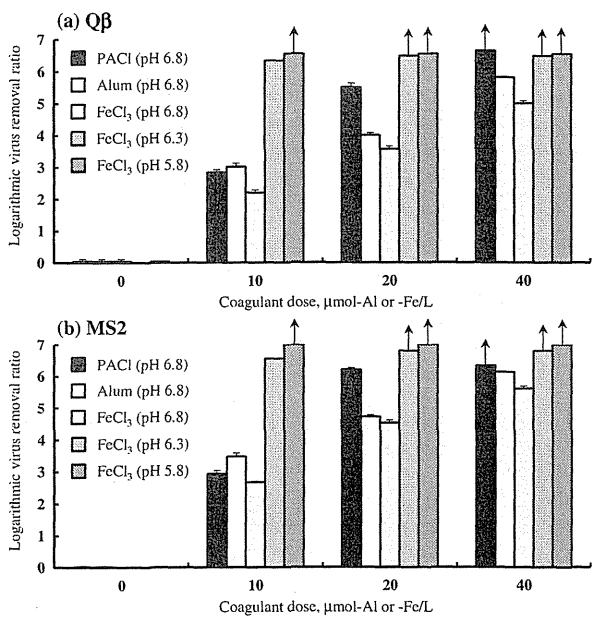

Fig. 6 – Bacteriophage removal by in-line coagulation followed by a ceramic microfiltration membrane having 0.1 μm diameter pores. The columns and error bars represent averages and standard deviations, respectively, of three runs. Arrows indicate virus concentrations below the quantification limit. (a) Qβ, (b) MS2.

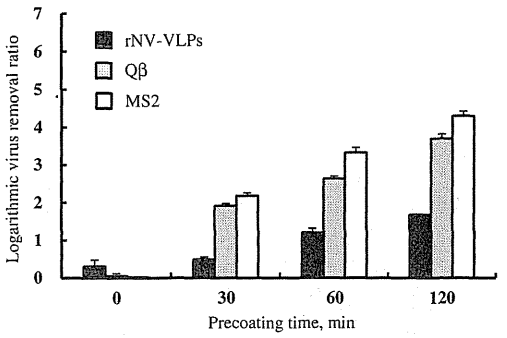

Fig. 7 – Virus removal by a ceramic MF membrane precoated with PACl (20 μmol-Al/L). No coagulant was used during the virus removal experiments. The columns and error bars represent averages and standard deviations, respectively, of three runs.